



UNIVERSITY OF LEEDS

This is a repository copy of *The study of structural, morphological and optical properties of (Al, Ga)-doped ZnO: DFT and experimental approaches*.

White Rose Research Online URL for this paper:
<http://eprints.whiterose.ac.uk/143993/>

Version: Accepted Version

Article:

Sikam, P, Moontragoon, P, Ikonic, Z et al. (2 more authors) (2019) The study of structural, morphological and optical properties of (Al, Ga)-doped ZnO: DFT and experimental approaches. *Applied Surface Science*, 480. pp. 621-635. ISSN 0169-4332

<https://doi.org/10.1016/j.apsusc.2019.02.255>

© 2019 Elsevier B.V. All rights reserved. Licensed under the Creative Commons Attribution-Non Commercial No Derivatives 4.0 International License (<https://creativecommons.org/licenses/by-nc-nd/4.0/>).

Reuse

This article is distributed under the terms of the Creative Commons Attribution-NonCommercial-NoDerivs (CC BY-NC-ND) licence. This licence only allows you to download this work and share it with others as long as you credit the authors, but you can't change the article in any way or use it commercially. More information and the full terms of the licence here: <https://creativecommons.org/licenses/>

Takedown

If you consider content in White Rose Research Online to be in breach of UK law, please notify us by emailing eprints@whiterose.ac.uk including the URL of the record and the reason for the withdrawal request.



eprints@whiterose.ac.uk
<https://eprints.whiterose.ac.uk/>

**The study of structural, morphological and optical properties of (Al, Ga)-doped ZnO:
DFT and experimental approaches**

Pornsawan Sikam¹, Pairot Moontragoon^{1,2,3*}, Zoran Ikonc⁴, Thanayut Kaewmaraya^{1,2},
Prasit Thongbai^{1,2}

¹Department of Physics, Khon Kaen University, Khon Kaen, 40002, Thailand.

²Integrated Nanotechnology Research Center (INRC), Department of Physics, Khon Kaen University, Khon Kaen, 40002, Thailand.

³Thailand Center of Excellence in Physics, Commission on Higher Education, Bangkok, 10400, Thailand.

⁴School of Electronic and Electrical Engineering, University of Leeds, Woodhouse Lane, Leeds LS2 9JT, United Kingdom.

*Corresponding author at: Department of Physics, Faculty of Science, Khon Kaen University, Khon Kaen, 40002, Thailand.

Tel.: +66 87 5149482; fax: +66 43 202374.

E-mail addresses mpairo@kku.ac.th (P. Moontragoon)

ABSTRACT

ZnO is widely studied for several applications such as a photocatalyst, a working electrode for dye-sensitized solar cells and for thermoelectric devices. This work studies the effect of an increase in the number of carriers by doping ZnO with Al and Ga. The 6.25 mol% of Al-doped ZnO, 6.25 mol% of Ga-doped ZnO, and 12.5 mol% of (Al, Ga) co-doped ZnO nanoparticles were prepared using combustion method. The prepared samples were then characterized by X-ray diffraction, transmission electron microscope, energy-dispersive X-ray spectroscopy and UV-visible spectroscopy techniques. Moreover, density functional theory (DFT) was also employed for computational studies of Al and Ga doped ZnO. Optimized structures, density of states (DOS) and band structures of these materials were calculated using Vienna Ab initio Simulation Package code. From this study, Al and Ga are found to play an important role in morphology and optical properties of the ZnO, changing the band gap and Fermi level of ZnO. Then, the prepared samples were characterised for their thermoelectric properties, and modelling of thermoelectric properties of ZnO, Al-doped ZnO, Ga-doped ZnO and (Al, Ga)-co doped ZnO was performed using BoltzTraP code. Furthermore, the Seebeck coefficient, electrical conductivity, relaxation time, electronic thermal conductivity and power factor were studied. The experimental and computational results are pointing in the same direction, that the thermoelectric properties of the ZnO are changed by doping: the semiconducting ZnO transforms into metallic ZnO when doped with Al and Ga. This leads to ZnO showing new thermoelectric properties, in particular the Ga-doped ZnO and (Al, Ga)-co doped ZnO: they provide high electrical conductivity and power factor. Therefore, it is expected that these good properties might promote the ZnO to be a potential candidate for applications, especially in high efficiency thermoelectric devices.

Keywords: Thermoelectric properties, DFT, Al-doped ZnO, Ga-doped ZnO, (Al-Ga)-co doped ZnO

1. Introduction

ZnO is a semiconductor which is cheap to synthesize using various methods such as hydrothermal [1], combustion [2], microemulsion [3] and sol-gel [4]. Because of the very simple routes to prepare the ZnO, there are a number of research efforts trying to apply it in various applications: solar cells [5], photocatalysts for degradation reaction [6, 7], transistors [8] and gas sensors [9]. In addition, in the last two decades the ZnO has attracted attention for its prospects to be used in thermoelectric devices [10-14]. An advantage of ZnO thermoelectric devices is that semiconductors are commonly known from theory to provide a larger Seebeck coefficient than metals. However, semiconductors have smaller electrical conductivity than metals. Thus, ZnO is a potential candidate for efficient thermoelectric devices. There is an exploration route to improve thermoelectric properties of ZnO by doping it with other atoms, so that one could engineer the band structure and improve thermoelectric properties of the host materials [2, 14, 15].

Briefly about the thermoelectric properties, the dimensionless figure of merit ZT is defined to be a thermoelectric performance indicator, where $ZT = (S^2\sigma T)/\kappa$ and S is the Seebeck coefficient, giving the voltage difference between two points per unit temperature difference, σ is the electrical conductivity, T the temperature and κ the thermal conductivity, where $\kappa = \kappa_e + \kappa_l$ where κ_e is the electronic thermal conductivity and κ_l is the lattice thermal conductivity or phonon thermal conductivity [11, 13].

In 1997, Tsubota et al. [11] reported that the power factor at 1000 °C of the ZnO is about $4 \times 10^{-4} \text{ Wm}^{-1}\text{K}^{-2}$ which is less than that of $\text{Zn}_{0.95}\text{Al}_{0.05}\text{O}$; it is about $13 \times 10^{-4} \text{ Wm}^{-1}\text{K}^{-2}$. Here, it is interesting to note that Al doping increases the power factor at higher temperature, compared to the pure ZnO. In the same direction as in the report of Ohtaki et al. [12], the ZT of $\text{Zn}_{0.98}\text{Al}_{0.02}\text{O}$ of around 0.2 was observed. However, there is an observed disadvantage: Tsubota et al. [11] found that there is decrease in magnitude of the Seebeck coefficient when Al is added into the ZnO structure. Moreover, an increase in electrical conductivity and the decrease in magnitude of the Seebeck coefficient when Al atoms were added into the ZnO are also shown by Qu et al. [10] and Jantrasee et al. [13]. In addition to Al doping, Ga is also used for doping ZnO. Khuili et al. [16] gave a computational result in 2016 that electrical conductivity of the Al-doped ZnO and Ga-doped ZnO shows larger values than that of the pure ZnO.

From this point, it is realized that adding other atoms into the host ZnO structure, especially Al and Ga, might enhance the thermoelectric performance of ZnO because introducing Al and Ga in ZnO increases the carriers density in the system, which is expected to increase electrical conductivity, because of electrons added in the ZnO. A following interesting question is on

how the thermoelectric properties of ZnO will be affected if the Al and Ga atoms are together doped into the ZnO; that is, co-doping of Al and Ga in ZnO. Thus, this work studies the effects of the Al and Ga doping on the structural, optical and thermoelectric properties of the ZnO host structure via experimental and first-principles calculation approaches. In the experiment, combustion method is chosen to synthesize the ZnO, Al-doped ZnO, Ga-doped ZnO and (Al, Ga)-doped ZnO because this synthesis is very simple and faster than other methods. Moreover, the density functional theory (DFT) study with generalized gradient approximation (GGA) is employed for computational study.

2. Experimental details

2.1 Synthesis details

The ZnO, $Zn_{1-x}Al_xO$, $Zn_{1-x}Ga_xO$ and $Zn_{1-2x}Al_xGa_xO$ ($x = 0.0625$) nanoparticles were synthesized using a combustion method. Firstly, $Zn(CH_3CO_2)_2$ was dissolved in deionized (DI) water. Next, $AlN_3O_9 \cdot 9H_2O$ solution was added into the ZnO solution with continuous stirring for the preparation of $Zn_{1-x}Al_xO$. After that, dissolved citric acid in ethanol and dissolved polyethylene glycol (PEG) in ethanol were mixed into the previous solution while being stirred continually. Then, the final solution was continuously stirred and heated at 220 °C. After the solution transform to gel, it was heated into an oven at 350 °C for an hour, combustion process. After cooling down, as-synthesized powder will be obtained. The next step is that the precursor would be calcined at 500 °C in normal atmosphere for 8-hours with heating rate 1 °C/minute. In case of $Zn_{1-x}Ga_xO$, $GaN_3O_9 \cdot xH_2O$ solution would be added instead of the $AlN_3O_9 \cdot 9H_2O$ solution and, both $GaN_3O_9 \cdot xH_2O$ and $AlN_3O_9 \cdot 9H_2O$ were added for the $Zn_{1-2x}Al_xGa_xO$.

2.2 Characterizations

Having calcined, the produced powders were characterized for their structure and examined for composition elements using X-ray diffraction technique (XRD, PANalytical, EMPYREAN) and energy-dispersive X-ray spectroscopy analysis (EDX, SEC, SNE-4500M), respectively. Then, the transmission electron microscopy (TEM) photographs and selected area electron diffraction (SAED) were studied via the transmission electron microscopy (FEI, TECNAI G² 20). Additionally, the optical band gap of prepared samples was examined by using UV-Vis spectroscopy (Shimadzu, UV-3101PC) in absorbance mode under ultraviolet and visible spectra radiation. Finally, synthesized powder was hot pressed and polished as bulk. Then, the Seebeck coefficient and electrical conductivity of prepared samples were found using TRC-ZTM2.

3. Computational details

First of all, a $2 \times 2 \times 2$ supercell of ZnO was used as initial model. This system contains 32 atoms, i.e. sixteen zinc atoms and sixteen oxygen atoms. In case of density of states (DOS), band structure and phonon calculation, Vienna Ab initio Simulation Package (VASP) [17] with Projector-augmented plane wave pseudopotential method (PAW) [18] were employed under the generalized gradient approximation (GGA) of the scheme of Perdew–Burke–Ernzerh (PBE) to treat exchange and correlation energy. In this calculation, 400 eV cutoff energy for plane waves was used, and the orbitals of Zn($d^{10} p^2$) and O($s^2 p^4$) were treated as valence electrons. After that, a Zn atom was replaced by Al and Ga atoms for Al-doped ZnO and Ga-doped ZnO, respectively. Moreover, two atoms of Zn were substituted by one atom of Al and one atom of Ga for (Al,Ga)-co doped ZnO. For Al and Ga, electrons in Al($s^2 p^1$) and Ga($s^2 p^1$) orbitals were treated as valence electrons. $5 \times 5 \times 3$ k-point meshes in the Brillouin zone were employed in optimization while $13 \times 13 \times 7$ of k-point grids were utilized to calculate DOS and band structures. The study of thermoelectric properties, $21 \times 21 \times 21$ of k-point grids were used for the calculation of thermoelectric properties under the semi-classical Boltzmann transport theory in BoltzTraP [10, 19-21].

4. Results and discussion

In the first step, total energy of Al and Ga substitution on Zn and O sites is calculated to examine which host atoms these doping atoms could replace. The calculated total energy of Al and Ga doping on the ZnO structure is presented in Table 1. Here, the substitution of Al and Ga atoms on the Zn sites shows a smaller total energy, compared to the O sites. This shows that the added Al and Ga might replace the Zn sites. Therefore, this work will study the pure ZnO and Zn-site substitution by Al and Ga named as undoped ZnO, $Zn_{1-x}Al_xO$, $Zn_{1-x}Ga_xO$ and $Zn_{1-2x}Al_xGa_xO$ ($x = 0.0625$).

Table 1 Total energy of the host site replacement with Al and Ga atoms.

Structures	Added atom	Replaced atom	Total energy (eV)
Al-doped ZnO			
	Al	Zn	-148.327
	Al	O	-133.823
Ga-doped ZnO			
	Ga	Zn	-144.831
	Ga	O	-133.640

After that, supercell of eight-times primitive cell of the ZnO, Al-doped ZnO, Ga-doped ZnO and $Zn_{1-2x}Al_xGa_xO$ are modelled and optimized. Fig. 1(a-c) shows the optimized structures. Lattice constants of these structures are given in Table 2. Comparing lattice constant of undoped ZnO to that of doped ZnO shows that the zinc-site substitution with Al and Ga atoms leads to distortion in the host structure. This is because of an ionic-radius inequality, that is 74.0, 53.5 and 62.0 pm for Zn^{2+} , Al^{3+} and Ga^{3+} , respectively. This result is according to the XRD results from the experiment, as shown in Fig. 2-3, because there are observed peak shifts in the XRD patterns after Al and Ga are added into the ZnO structure. These shifting peaks indicate the distortion in the structure following Bragg's equation of $2d\sin\theta = n\lambda$ where d is the plane distance, θ the incidence angle of incident X-ray beam, n the integer and λ the wave length of incident X-rays [22].

Table 2 Computed lattice parameters of supercell-size structures of the ZnO, Al-doped ZnO, Ga-doped ZnO and (Al, Ga)-co doped ZnO.

Structures	Lattice parameters				
	a (Å)	c (Å)	alpha (°)	beta (°)	gamma (°)
ZnO	6.5082	10.4717	90.0000	90.0000	120.0403
Al-doped ZnO	6.4987	10.4840	90.0005	89.9995	120.0361
Ga-doped ZnO	6.5149	10.5063	89.9999	90.0001	120.0358
(Al, Ga)-co doped ZnO	6.5031	10.5256	90.0005	89.9995	120.0354

Overall, the ZnO, Al-doped ZnO, Ga-doped ZnO and (Al, Ga)-co doped ZnO were successfully synthesized using the combustion method in the experimental part. All prepared samples show hexagonal wurtzite structure of ZnO (ICDD: 36-1451) as the main phase, as seen in Fig. 2. Comparing the as-prepared and calcined samples, calcination makes the observed peaks sharper. That is, the heat treatment leads to more regular atomic arrangement. Nonetheless, an existence of the added Al and Ga contents is confirmed by the EDX analysis, as shown in Fig. 4. The presented data is an elemental composition as a relative percentage.

In addition to success in the doping Al and Ga on the ZnO structure, nanoparticles are obtained as well, as seen in Fig. 5. From the TEM images it follows that particle size changes, from an average size around 80-100 nm to 20-40 nm, by the added Al and Ga contents. The smaller particle size and shape edge might be caused by the reduced structural formation, compared to the undoped ZnO. This is because the added atoms might inhibit the wurtzite structural formation of Zn and O, leading to some defects in the structures, and decrease the particle size. Moreover, the crystal planes of the ZnO wurtzite structure are observed in all prepared samples, as seen in SAED patterns in Fig. 5.

Moving to the calculation aspects, Fig. 6 shows the total DOS (TDOS) of the undoped ZnO, Al-doped ZnO, Ga-doped ZnO and (Al, Ga)-co doped ZnO, computed using $13 \times 13 \times 7$ k-point grids. Comparing TDOS of the doped to the undoped ZnO, there is a shift of the valence band maximum from 1.13 eV for the ZnO to 1.32 eV for the Ga-doped ZnO, 1.40 eV for the co-doped system and 1.41 eV for the Al doping. This might affect the band gap and band edge of the materials, and it also might affect their thermoelectric properties (TE). However, more details concerning the optical properties will be discussed later. In addition, upwards shift of the Fermi level (E_f) is also observed. In the ZnO, the E_f is positioned at the highest states of valence band, while in the doped system the E_f locates in the conduction band, according to the report of Jantrasee et al. and Khuili et al. [13, 16]. This point indicates that adding Al and Ga atoms in the ZnO structure leads to shift of Fermi level upwards, because the Zn^{2+} site substitution with Al^{3+} and Ga^{3+} is the n-type doping; i.e. more free electrons will be generated from donor states, resulting in the shifting of the E_f state to higher level (in the conduction band). This point is important because the Fermi level affects the TE properties [14].

Partial DOS and projected DOS, as shown in Fig. 6-10, will be considered next. For the undoped ZnO, the maximum state is occupied by Zn and O carriers, d-orbital electrons of Zn and p-orbital electrons of O, according to the report of Hachimi et al. [23]. After that, when Al and Ga atoms are added into the ZnO structure, there are new states observed above the 1.13 eV, as previously seen in the total DOS. From the Fig. 10, the interaction in the highest states

of doped systems results from d-orbital for Zn, o-orbital for O, p-orbital for Al and d-orbital for Ga. Moreover, comparing the projected DOS graphs of Zn and O in the doped systems to that for the undoped system, the Zn and O show different DOS, especially in the top of valence band. Therefore, it could be claimed that new states in the top of valence band come from interaction of Al and Ga with the nearest neighbor atom, Zn and O. Here, it is seen that adding Al and Ga on the ZnO could engineer DOS of the ZnO, which might lead to appreciating its optical and TE properties. This result is according to the report of Khuili et al. [16].

Another evidence presenting the difference of the ZnO and doped ZnO is their band structure. Here, the band-structures of supercell models are computed using band-structure code [24, 25] and shown in Fig. 11-12. Three-dimensional plots have the wave vector on the x axis, the $\epsilon - \epsilon_F$ on the y axis and, the electron density on the z axis; represented by color from the minimum value of blue (zero) to the maximum value of red. Here, ZnO shows direct band gap because the maximum valence band and minimum conduction band are at the same Γ point, in agreement with the literature, e.g. Honglin et al. and Mohamad et al. [26, 27]. Gap between valence band and conduction band (E_g) is 0.76 eV. Moreover, there is light electron density at the top of valence band. It is possible that electron hopping probability from the valence band to the conduction band in pure ZnO may be smaller than in the doped ZnO. This is due to the fact that all doped systems show heavy electron density on the top of valence band, almost twice as large as the electron density. Additionally, not only the ZnO, but also all doped materials show the direct band gap behavior. As for the band gap width, the E_g is 0.60, 0.53 and 0.64 eV for the Al doping, Ga substitution and co-doped ZnO structures, respectively.

Then, the band gap of prepared samples will be discussed next. Graphs of photon energy and $(\alpha h\nu)^2$ are illustrated in Fig. 13, where α is the absorption coefficient, h the Planck's constant and ν the photon frequency. This plot follows an equation of $\alpha h\nu = k(h\nu - E_g)^{n/2}$ when k and n are constants, where n would be 1 and 4 for direct and indirect band gap materials, respectively [28, 29]. From the results, ZnO shows the band gap of 3.18 eV while the E_g of the doped systems is 3.18, 3.15 and 3.16 eV for Al-doped ZnO, Ga-doped ZnO and (Al, Ga)-co-doped ZnO, respectively. Comparing the DFT band structures to the optical band gap obtained from the experiment, there is a considerable difference of obtained band gaps from these two approaches. The large underestimate of the value of E_g obtained from the DFT study is caused by unrealistic interaction force of electron-electron, electron-nucleus and nucleus-nucleus interaction, due to limitations of the DFT calculation. However, the DFT is employed in this work because less resources are required in calculation compared to Hartree-Fock approximation. Although the obtained band gap from the first-principles calculation is not

equal to the experimental result, it can provide important evidences; this is what happens when the Zn sites are replaced by Al and Ga atoms, such as partial DOS, projected DOS and electronic band structures. However, an essential point of the band gap of these material is that band gap of the doped ZnO is wider than that of the undoped ZnO. From this point, it is good for the photocatalyst application of the ZnO because narrower band gap after Al and Ga adding could support photocatalytic performance under the Sun radiation. Thus, it is possible that the Al and Ga doping of the ZnO structure could organize the electron-occupied energy level and band structure of the ZnO which might lead to the change in optical and thermoelectric properties of the ZnO. Since electrons are fermions, the probability of occupying any energy level is given by Fermi-Dirac distribution, the electron distribution will be a function of the E_f and the Seebeck coefficient depends on both the E_g and E_f of semiconductor materials [30]. Thus, if there is change in both E_f and E_g when the Al and Ga were added into the ZnO, as shown in the calculation results, it is possible that Al and Ga doping on the ZnO might improve the TE properties of the ZnO.

Nevertheless, there is an option to correct the band gap in first-principles calculation. This is by adding Hubbard parameter for d-orbital elements. The Hubbard parameter will be added to adjust the interaction of d-orbital electrons. Here, the Hubbard parameter of U_{eff} as 9.0 eV ($U=10.0$ eV and $J= 1.0$ eV) and 7.0 eV is employed for Zn and Ga, respectively, following the report of Jantrasee et al. [13] and Dong et al. [31]. In this work, the GGA+U using k-point meshes of $21 \times 21 \times 21$ for the ZnO and $13 \times 13 \times 7$ for the doped systems will be employed to calculate thermoelectric properties of undoped ZnO and doped ZnO because the Fermi level of the doped systems is at conduction band already for $13 \times 13 \times 7$ k-point grids. DOS of these systems are calculated and shown in Fig 14-15. From the DOS, it is seen that the E_f of the materials sits near the conduction band. The appearance of the E_f under the minimum conduction band indicates that these materials should be n-type semiconductors due to majority carriers being electrons, they generate donor states in the forbidden band, resulting in shift of E_f from the middle gap for undoped semiconductors to the near conduction band for n-type materials. The next step is to use the output data from these calculations for the thermoelectric properties.

Thermoelectric properties calculated using BoltzTraP code for the ZnO and doped ZnO are shown in Fig 16. From the graphs, the zinc oxide shows the negative value with magnitude of Seebeck coefficient around 242 $\mu\text{V/K}$. This result is in accordance with the experimental reports of Tsubota et al. and Qu et al. [10, 11]. Then, electronic thermal conductivity tends to slightly increase with increasing temperature, corresponding to the reported results of Qu et al. [10]. Comparing the doped ZnO to the pure ZnO, magnitude of the Seebeck coefficient of the doped systems is obviously smaller than that of the pure ZnO, while electric conductivity per relaxation time and electronic thermal conductivity per relaxation time of the doped ZnO are higher than that of the pure ZnO. It is clear that Al and Ga doping of the ZnO could improve electrical conductivity of the ZnO, according to the report of Khuili et al. and Qu et al. [10, 16].

Moving to consider experimental parts, the plots of the thermoelectric properties of the synthesized undoped ZnO and doped ZnO are shown in Fig. 17. The ZnO illustrates negative value of the Seebeck coefficient with magnitude in range from about 70 to 128 $\mu\text{V/K}$. Comparing the doped to the undoped ZnO, the decrease in magnitude of the Seebeck coefficient of the ZnO with temperature increase is observed, while all the doped ZnO materials show a larger magnitude with increasing temperature. Moreover, the doped ZnO shows negative value of the Seebeck coefficient, similar to the undoped ZnO. However, the magnitude of the Seebeck coefficient of the Al-doped ZnO is smaller than that of ZnO. From this point, the observed experimental results are in accordance with the obtained computational results.

In case of the electrical conductivity σ , the ZnO shows trend to increase with increasing temperature, which is the same trend to the Al-doped ZnO; this trend is according to the calculated result and report of the Qu et al. [10]. Nonetheless, the value of the electrical conductivity of the Al-doped ZnO is a bit larger than that of the ZnO. For Ga-doped ZnO and (Al, Ga)-doped ZnO, their electrical conductivity decreases with temperature increasing from room temperature to 1000 K. However, it is still much larger than for the ZnO and Al-doped ZnO. Both Ga-doped ZnO and (Al, Ga)-doped ZnO show a much appreciated electrical conductivity because their electrical conductivity is very large compared to undoped ZnO and Al-doped ZnO. From this result one can infer that Ga doping and cooperation of Al and Ga could change semiconductor ZnO to be a metallic ZnO with high σ .

Considering the electrical conductivity of the prepared samples and the calculation result, obtained using BoltzTraP code (σ/τ), it is assumed that at the same temperature, their electrical conductivity would be the same. In this work, difference of the temperature of the

experiment and calculation is different up to 6.0 K. Therefore, electrical conductivity σ of the DFT calculation will be as shown in Fig. 18(up). After that, the relaxation time τ of materials in Fig. 16 could be calculated using the electrical conductivity from Fig. 18(up). Then, the relaxation time will be obtained as seen in Fig. 18(down). Here, it is seen that the ZnO shows the largest value of the relaxation time. Their relaxation time is decreasing with temperature increasing from 5.77 to 1.77×10^{-15} s for the temperature from 300 to 1000 K. This might be because heating could lead carriers to have smaller relaxation time. This relaxation time is not much smaller than that in the report of Ozgur et al., the reported 17×10^{-15} s for carrier concentration of the order of 10^{16} cm^{-3} [32]. In case of doped ZnO, their relaxation time is much smaller, compared to the ZnO. It might be due to their metallic behavior. This is because there are more electrons there than in the undoped ZnO.

Next, the electronic thermal conductivity κ_e will be obtained from the κ_e/τ , using the values of τ in Fig. 18(down). The obtained κ_e are shown in Fig. 19(up). Additionally, the κ_e is calculated using Wiedemann-Franz law of $\kappa_e = L\sigma T$ where L is the Lorenz factor ($2.45 \times 10^{-8} \text{ V}^2/\text{K}^2$), σ the electrical conductivity and T the temperature [13, 33]. The σ is in Fig. 18(up). Here, the obtained κ_e from two approaches almost equal. From the results, it is seen that ZnO and Al-doped ZnO show very low electronic thermal conductivity while Ga doping and co doping have the large κ_e . Thus, Ga doping and (Al, Ga)-co doping on the ZnO could promote both electrical and electronic conductivity of the ZnO because both properties come from electron motion, conducting both electricity and heat.

Finally, ability to transform heat to electrical energy of the prepared materials is studied via power factor P, where $P = S^2\sigma$, where S is the Seebeck coefficient and σ the electrical conductivity. Fig. 20(up) shows the graphs of power factor of the synthesized ZnO and doped ZnO. Here, the power factor of the ZnO drops with temperature increase, which points out that ability of ZnO to convert heat to electrical energy will decrease when it is used at higher temperature. Nevertheless, an appreciated result is observed in the doped ZnO. The all doped ZnO materials show greater power factor with temperature increase, especially Ga and (Al, Ga)-co doped ZnO. This point is very interesting because it points out that Ga doping and (Al, Ga)-co doping on the ZnO can improve the power factor of the ZnO and it gives much better results than only Al-doped ZnO. In case of the Fig. 20(down), it is showing the power factor obtained results from the DFT calculation. The massive power factor of the ZnO is observed. This might be due to the fact that the Seebeck coefficient of the ZnO in Fig. 16 is very large compared to the doped systems, about 10 times. Additionally, to calculate the power factor, the

Seebeck coefficient will be squared. Thus, the power factor of the ZnO should be about 100 times larger, compared to the doped ZnO. However, the possible reason that the power factor of the ZnO is not 100 times larger than that of the doped ZnO is that electrical conductivity of the doped ZnO is greater than the undoped ZnO. However, the difference of the calculation and experimental results might come from the assumption that electrical conductivity of the DFT calculation is equal to that of the experiment. Another reason is the temperature difference of the calculation results and the experimental result as mentioned above. Moreover, the employed parameters in calculations, such as Hubbard parameter U and number of k -points, might effect to the obtained results as well. Nonetheless, it cannot be denied that calculation approach is still important because it can provide predictive guidelines and answer many questions about experimental results.

From the thermoelectric properties obtained in this study of the undoped and doped ZnO, it is possible that more electron carriers in the ZnO, when Al and Ga were added, results in metallic behavior of the ZnO. The number of electron carriers is similar to Electron Sea, leading to metallic behavior of the ZnO. Metals always show higher electrical conductivity than the semiconductors, while the magnitude of Seebeck coefficient of the semiconductor is greater than that of the metals. From this study, ZnO semiconductor, which shows large values of Seebeck coefficient and very small electrical conductivity per relaxation time, transforms to metallic ZnO, with smaller Seebeck coefficient, and with huge electrical conductivity and large power factor, when Al and Ga were doped into the structure. This is due to the fact that the Seebeck coefficient depends on the voltage difference of two points per temperature difference, as mentioned above, and $V=IR$ where V is the potential difference between two points, I the current flowing through the resistance and R the resistance, obeying Ohm's law. Thus, the higher electrical conductivity is, the smaller is the Seebeck coefficient. This causes a decrease of the Seebeck coefficient and ZT when Al and Ga are added into the ZnO. From this point, it is clear that adding Al and Ga could change thermoelectric properties of the ZnO from the semiconductor behavior to the metallic behavior with the very large electrical conductivity and power factor.

5. Conclusions

In this work, structural, optical and thermoelectric properties of the ZnO, Al-doped ZnO, Ga-doped ZnO and (Al, Ga)-co doped ZnO were studied via experimental and first-principles calculation approaches. In experiment, nanoparticles of ZnO, Al-doped ZnO, Ga-doped ZnO and (Al, Ga)-co doped ZnO are synthesized using combustion method. The results

from the XRD and SAED analysis confirm that main phase of the prepared samples is the wurtzite structure without any secondary phases observed. Additionally, the DFT study with GGA approximation is used via VASP code for calculating the supercells of these materials. From the study, it is seen that the Al and Ga adding on the ZnO structures enables one to engineer the ZnO's band structure. There are new states at top of valence band which come from interaction of valence electrons of Zn, O, Al and Ga atoms. The change in band structures and DOS of the ZnO after Al and Ga are added into the structures indicates that the dopant systems would show the impressive optical and thermoelectric properties. In this work, the synthesized Ga-doped ZnO and (Al, Ga)-co doped ZnO materials could significantly improve the thermoelectric properties of the ZnO, especially electrical conductivity and power factor. Here, it is possible that they would be potential candidates to be thermoelectric materials for high performance thermoelectric devices, because they could be synthesized using not very complex routes, and they can provide a very high power factor. Additionally, another observed benefit is that the calculated results agree well with experimental results. Therefore, great properties observed in the calculated results of the ZnO and doped ZnO could be examined in the real materials, not only in the simulation.

Acknowledgments

Funding for this work is provided by Thailand Research Fund under Grant No. RTA5680008, Integrated Nanotechnology Research Center (INRC), Khon Kaen University, Thailand, the Nanotechnology Center (NANOTEC), NSTDA, Ministry of Science and Technology, Thailand, through its program of Center of Excellence Network, Science Achievement Scholarship of Thailand (SAST).

References

1. Edalati, K., et al., Low-temperature hydrothermal synthesis of ZnO nanorods: Effects of zinc salt concentration, various solvents and alkaline mineralizers. *Materials Research Bulletin*, 2016. **74**: p. 374-379.
2. Sikam, P., et al., Structural, Optical, Electronic and Magnetic Properties of Fe-Doped ZnO Nanoparticles Synthesized by Combustion Method and First-Principle Calculation. *Journal of Superconductivity and Novel Magnetism*, 2016. **29**(12): p. 3155-3166.
3. Wang, Y., et al., Synthesis of ZnO nanoparticles from microemulsions in a flow type microreactor. *Chemical Engineering Journal*, 2014. **235**: p. 191-197.
4. Hasnidawani, J.N., et al., Synthesis of ZnO Nanostructures Using Sol-Gel Method. *Procedia Chemistry*, 2016. **19**: p. 211-216.

5. Huang, J., Z. Yin, and Q. Zheng, Applications of ZnO in organic and hybrid solar cells. *Energy & Environmental Science*, 2011. **4**(10): p. 3861-3877.
6. Lee, K.M., et al., Recent developments of zinc oxide based photocatalyst in water treatment technology: A review. *Water Research*, 2016. **88**: p. 428-448.
7. Chen, X., et al., Preparation of ZnO Photocatalyst for the Efficient and Rapid Photocatalytic Degradation of Azo Dyes. *Nanoscale Research Letters*, 2017. **12**(1): p. 143.
8. Xu, X., et al., Low-voltage zinc oxide thin-film transistors with solution-processed *channel and dielectric layers below 150 °C*. *Applied Physics Letters*, 2012. **101**(22): p. 222114.
9. Biasotto, G., et al., Gas sensor applications of zinc oxide thin film grown by the polymeric precursor method. *Ceramics International*, 2014. **40**(9, Part B): p. 14991-14996.
10. Qu, X., et al., Thermoelectric properties and electronic structure of Al-doped ZnO. *Solid State Communications*, 2011. **151**(4): p. 332-336.
11. Tsubota, T., et al., Thermoelectric properties of Al-doped ZnO as a promising oxide material for high-temperature thermoelectric conversion. *Journal of Materials Chemistry*, 1997. **7**(1): p. 85-90.
12. Ohtaki, M., et al., High - temperature thermoelectric properties of $(Zn_{1-x}Al_x)O$. *Journal of Applied Physics*, 1996. **79**(3): p. 1816-1818.
13. Jantrasee, S., S. Pinitsoontorn, and P. Moontragoon, First-Principles Study of the Electronic Structure and Thermoelectric Properties of Al-Doped ZnO. *Journal of Electronic Materials*, 2014. **43**(6): p. 1689-1696.
14. Sikam, P., et al., Enhanced thermoelectric properties of N-doped ZnO and SrTiO₃: A first-principles study. *Applied Surface Science*, 2018. **446**: p. 47-58.
15. Sikam, P., et al., DFT calculation and experimental study on structural, optical and magnetic properties of Co-doped SrTiO₃. *Applied Surface Science*, 2018. **446**: p. 92-113.
16. Khuili, M., et al., Comparative first principles study of ZnO doped with group III elements. *Journal of Alloys and Compounds*, 2016. **688**: p. 368-375.
17. Kresse, G. and J. Furthmüller, Efficiency of ab-initio total energy calculations for metals and semiconductors using a plane-wave basis set. *Computational Materials Science*, 1996. **6**(1): p. 15-50.
18. Blöchl, P.E., Projector augmented-wave method. *Physical Review B*, 1994. **50**(24): p. 17953-17979.
19. Madsen, G.K.H. and D.J. Singh, BoltzTraP. A code for calculating band-structure dependent quantities. *Computer Physics Communications*, 2006. **175**(1): p. 67-71.
20. Jantrasee, S., P. Moontragoon, and S. Pinitsoontorn, Optical and magnetic properties of doped ZnO: Experimental and simulation. *Journal of Optoelectronics and Advanced Materials*, 2016. **18**(11-12): p. 1033-1039.
21. Jantrasee, S., P. Moontragoon, and S. Pinitsoontorn, Thermoelectric properties of Al-doped ZnO: Experiment and simulation. *Journal of Semiconductors*, 2016. **37**(9).
22. The reflection of X-rays by crystals. *Proceedings of the Royal Society of London. Series A*, 1913. **88**(605): p. 428.
23. Hachimi, A.G.E., et al., First-principles prediction of the magnetism of 4f rare-earth-metal-doped wurtzite zinc oxide. *Journal of Rare Earths*, 2014. **32**(8): p. 715-721.
24. Medeiros, P.V.C., S. Stafström, and J. Björk, Effects of extrinsic and intrinsic perturbations on the electronic structure of graphene: Retaining an effective primitive cell band structure by band unfolding. *Physical Review B*, 2014. **89**(4): p. 041407.

25. Medeiros, P.V.C., et al., Unfolding spinor wave functions and expectation values of general operators: Introducing the unfolding-density operator. *Physical Review B*, 2015. **91**(4): p. 041116.
26. Li, H., et al., First-principles study of p-type conductivity of N-Al/Ga/In co-doped ZnO. *Physica Scripta*, 2015. **90**(2): p. 025803.
27. Mohamad, A.A., et al., First-principles calculation on electronic properties of zinc oxide by zinc–air system. *Journal of King Saud University - Engineering Sciences*, 2017. **29**(3): p. 278-283.
28. Zhang, L., et al., Rapid synthesis of ultrafine $K_2Ln_2Ti_3O_{10}$ (Ln=La, Nd, Sm, Gd, Dy) series and its photoactivity. *Journal of Solid State Chemistry*, 2005. **178**(3): p. 761-768.
29. Liu, C., et al., Influence of Fe-doping on the structural, optical and magnetic properties of ZnO nanoparticles. *Journal of Magnetism and Magnetic Materials*, 2012. **324**(20): p. 3356-3360.
30. Azároff, L.V. and J.J. Brophy, *Electronic processes in materials*. 1963: McGraw-Hill.
31. Dong, L., et al., Effects of oxygen vacancies on the structural and optical properties of β -Ga₂O₃. *Scientific Reports*, 2017. **7**: p. 40160.
32. Özgür, Ü., et al., A comprehensive review of ZnO materials and devices. *Journal of Applied Physics*, 2005. **98**(4): p. 041301.
33. Scott, J.F., H.G. Bohn, and W. Schenk, Ionic Wiedemann–Franz law. *Applied Physics Letters*, 2000. **77**(16): p. 2599-2600.

LIST OF FIGURE CAPTIONS

- Fig. 1** $2 \times 2 \times 2$ supercell of (a) ZnO, (b) Al-doped ZnO, (c) Ga-doped ZnO and (d) (Al, Ga)-co doped ZnO where grey balls as the zinc atoms, red the oxygen, blue the aluminum and green the gallium.
- Fig. 2** XRD patterns of as-prepared and calcined samples.
- Fig. 3** XRD patterns in range from 35.75 to 37.25 degree of 2theta of samples calcined at 500 °C.
- Fig. 4** Elemental composition of (a) undoped ZnO, (b) Al-doped ZnO, (c) Ga-doped ZnO and (d) (Al, Ga)-co doped ZnO calcined at 500 °C.
- Fig. 5** (left) TEM images and (right) SAED patterns of undoped ZnO, Al-doped ZnO, Ga-doped ZnO and (Al, Ga)-co doped ZnO calcined at 500 °C.
- Fig. 6** Total DOS calculated using the GGA scheme of the PBE of (a) ZnO, (b) Al-doped ZnO, (c) Ga-doped ZnO and (d) (Al, Ga)-co doped ZnO where Fermi level (E_f) is at 1.13, 3.82, 3.67 and 4.39 eV, respectively.
- Fig. 7** Total and partial DOS calculated by the GGA approximation of the ZnO where the E_f is at 1.13 eV, along dash line.
- Fig. 8** Total and partial DOS of (a) Al-doped ZnO and (b) Ga-doped ZnO when the E_f is addressed by dash line, locating at 3.82 and 3.67 eV for the Al-doped ZnO and Ga-doped ZnO, respectively, computed by the DFT with GGA method.
- Fig. 9** Obtained total and partial DOS from the calculation of DFT with GGA approach of (Al, Ga)-co doped ZnO with the dash line of E_f at 4.39 eV
- Fig. 10** Projected DOS calculated by the GGA approximation of (a) ZnO, (b) Al-doped ZnO, (c) Ga-doped ZnO and (d) (Al, Ga)-co doped ZnO.
- Fig. 11** Band structures, computed by the GGA scheme, of (a) ZnO, (b) Al-doped ZnO and (c) Ga-doped ZnO.
- Fig. 12** Band structure of (Al, Ga)-co doped ZnO obtained from the first-principles calculation method with GGA approximation.
- Fig. 13** Optical band gap of (a) ZnO, (b) Al-doped ZnO, (c) Ga-doped ZnO and (d) (Al, Ga)-co doped ZnO: experimental results.
- Fig. 14** DOS and band structure of primitive ZnO calculated using HSE calculation.
- Fig. 15** DOS calculated using GGA+U approach of (a) $21 \times 21 \times 21$ k-point meshes of ZnO and, $13 \times 13 \times 7$ k-point meshes of (b) Al-doped ZnO, (c) Ga-doped ZnO and (d) (Al, Ga)-

doped ZnO where the E_f is at 1.96, 3.82, 3.63 and 4.37 eV for the ZnO, Al-doped ZnO, Ga-doped ZnO and (Al, Ga)-co doped ZnO, respectively.

Fig. 16 (a) Total DOS and partial DOS and, (b) projected DOS of the (left) Zn and (right) O of the ZnO computed using k-point meshes of $21 \times 21 \times 21$ using GGA+U scheme.

Fig. 17 Thermoelectric properties calculated by BoltzTraP code of (a) Seebeck coefficient, (b) electrical conductivity divided by relaxation time and (c) electronic thermal conductivity per relaxation time of ZnO, Al-doped ZnO, Ga-doped ZnO and (Al, Ga)-co doped ZnO.

Fig. 18 Thermoelectric properties of (a) Seebeck coefficient and (b) electrical conductivity σ of prepared materials.

Fig. 19 (up) Electrical conductivity σ and (down) relaxation time: calculation part.

Fig. 20 Electronic thermal conductivity obtained from (up) BoltzTraP code and (down) Wiedemann-Franz law: calculation part.

Fig. 21 Power factor of ZnO, Al-doped ZnO, Ga-doped ZnO and (Al, Ga)-co doped ZnO: (up) experiment part and (down) DFT part.

Fig. 1

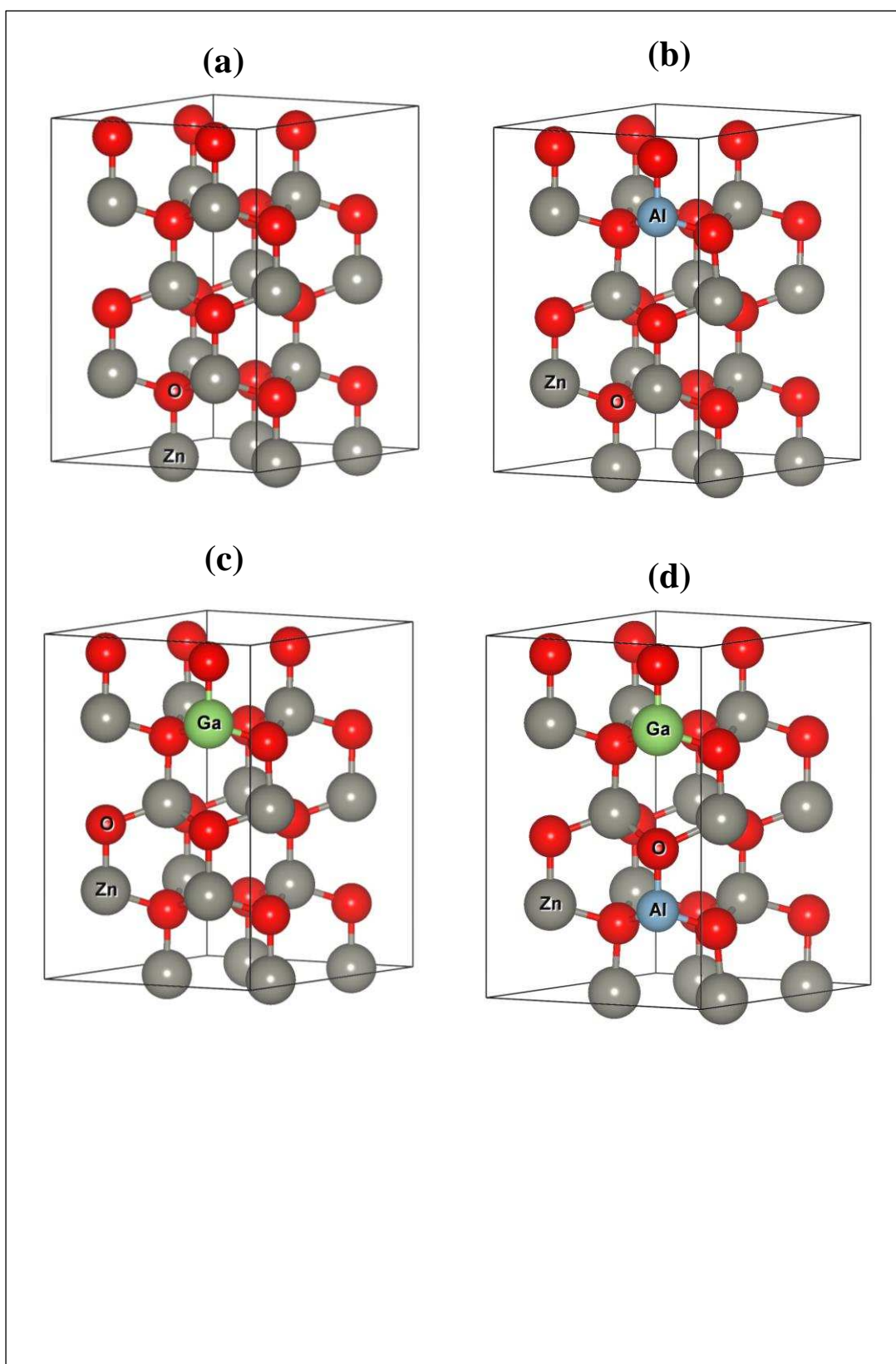


Fig. 2

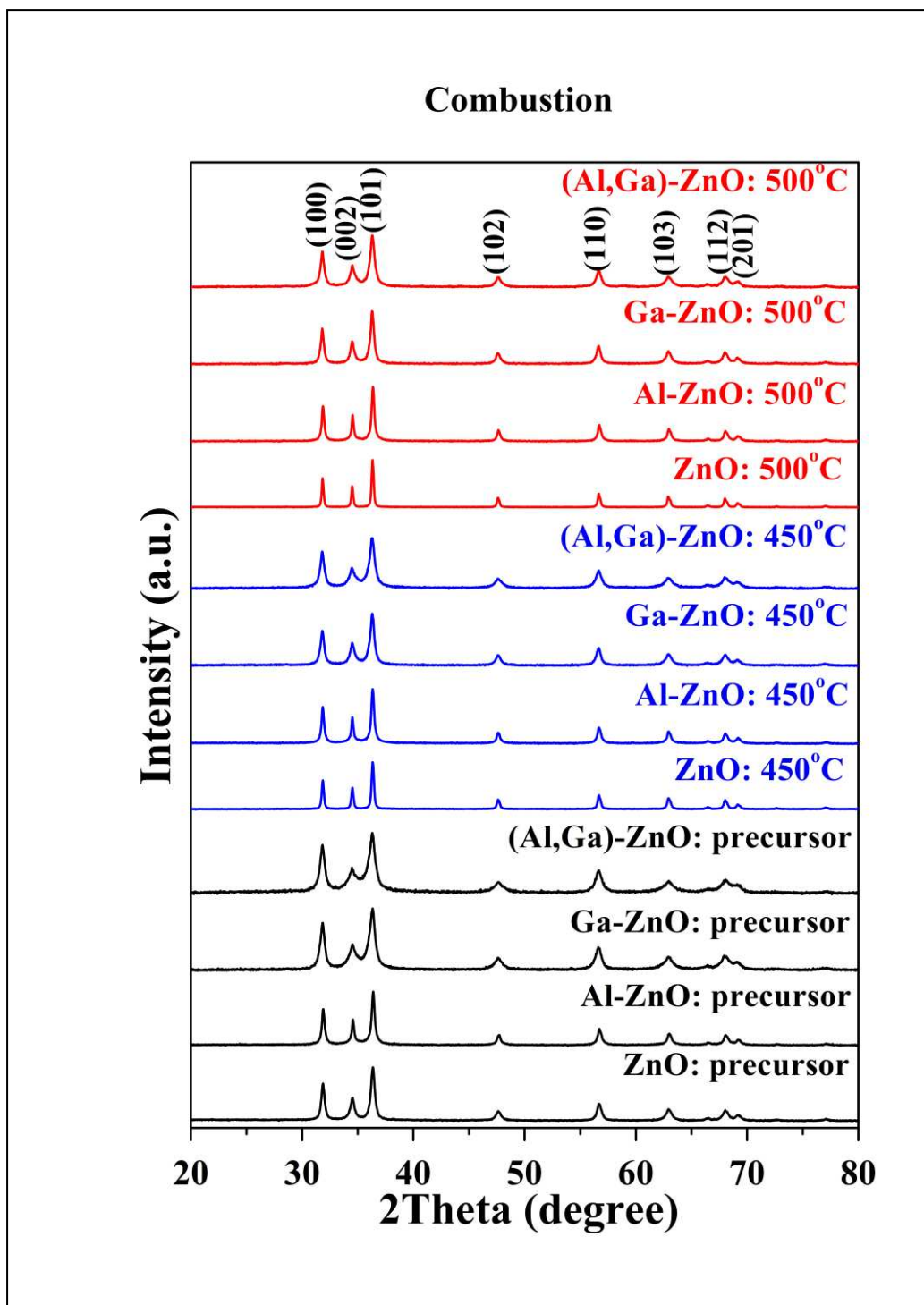


Fig. 3

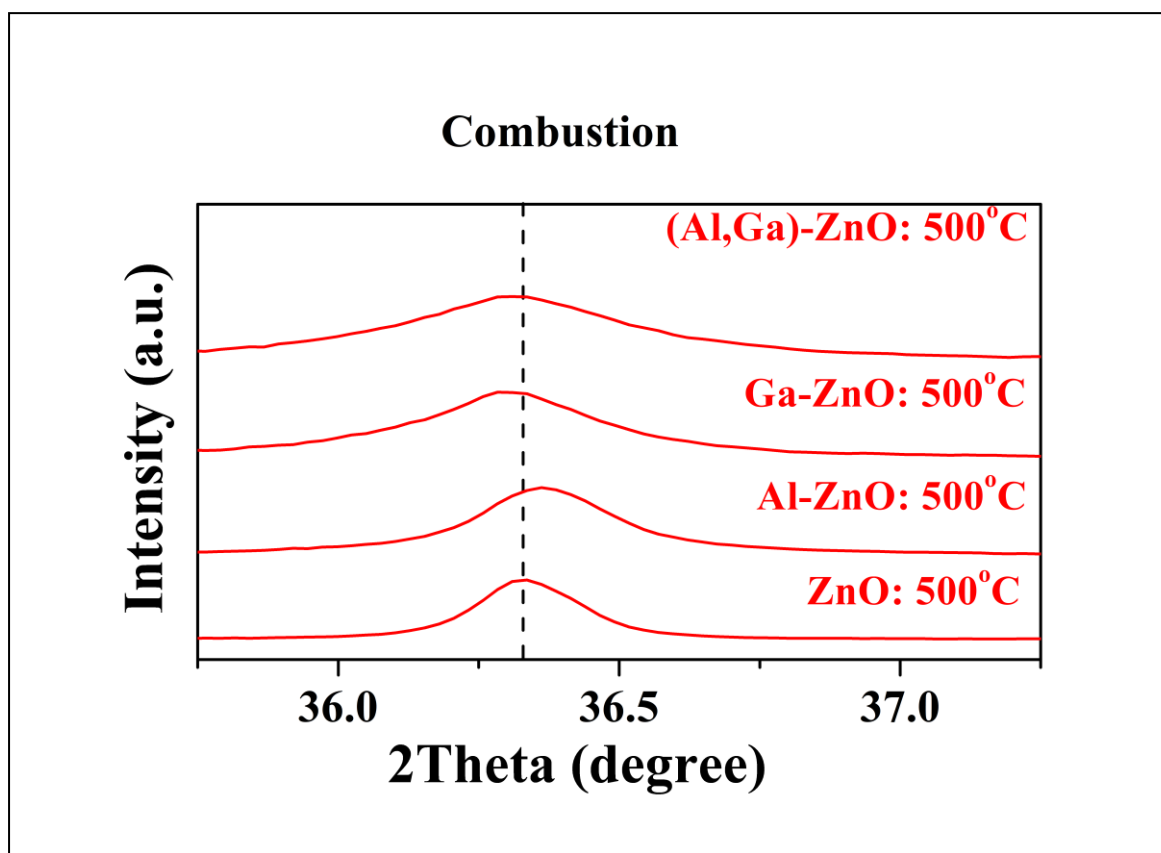


Fig. 4

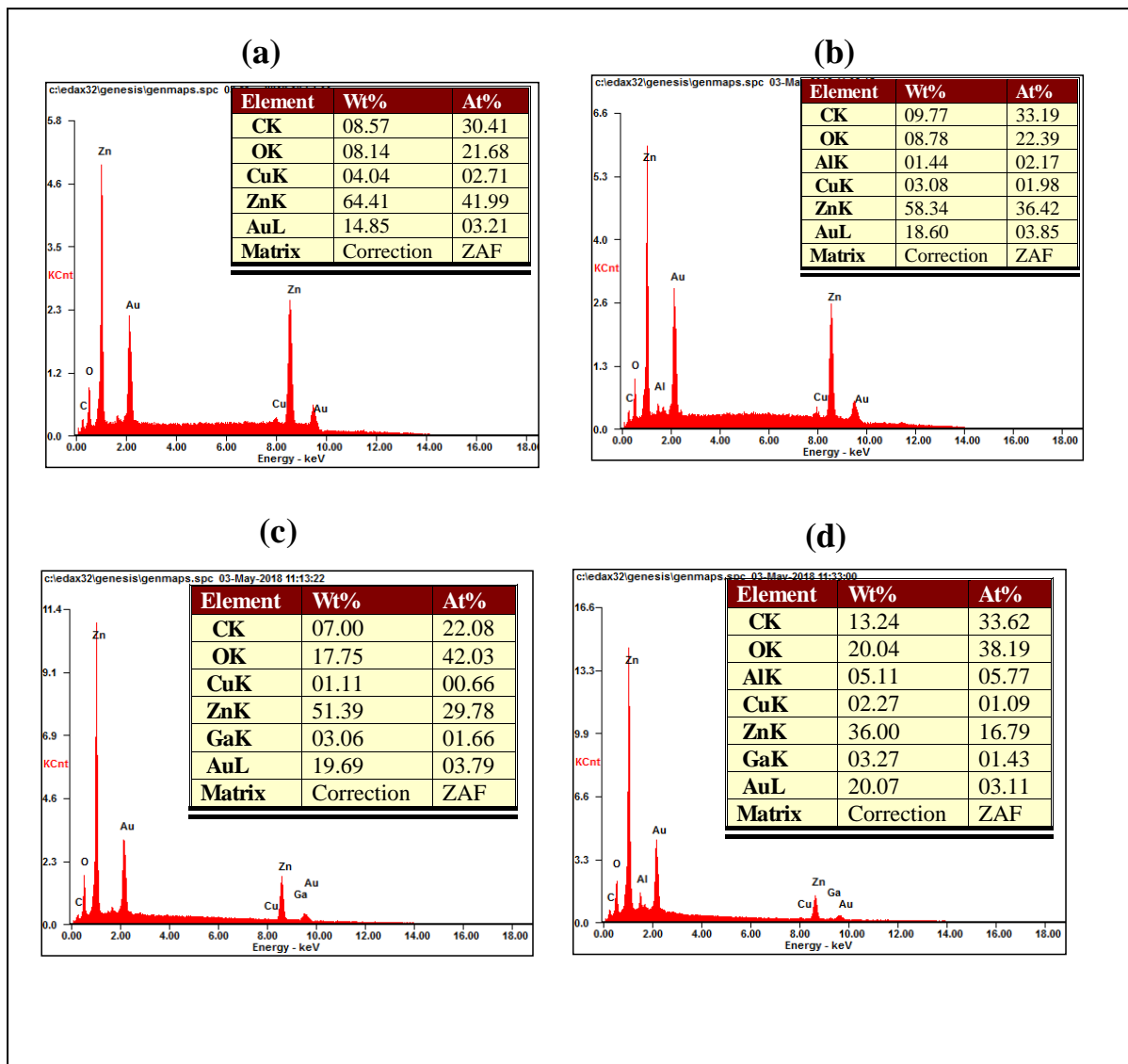


Fig. 5

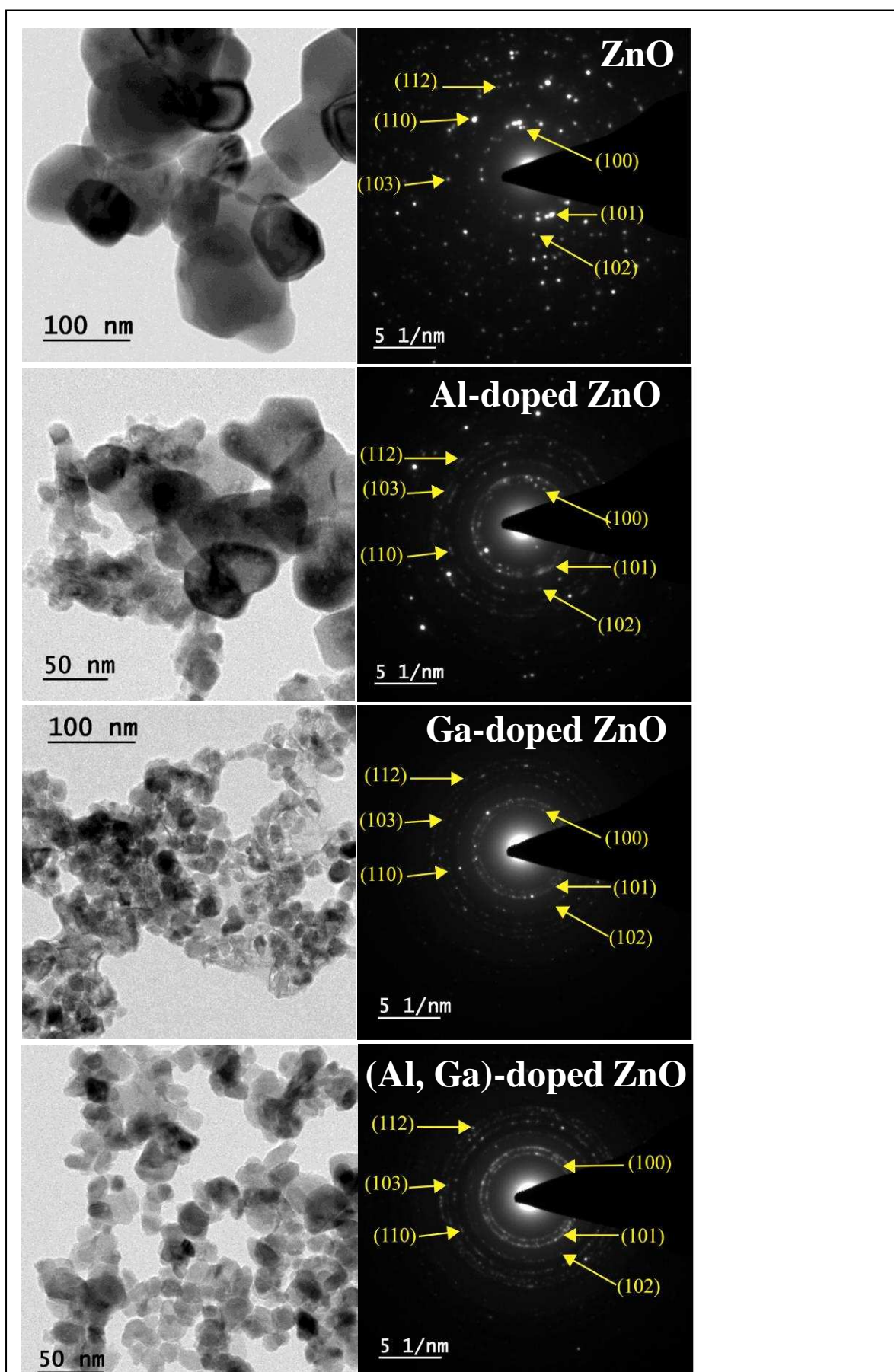


Fig. 6

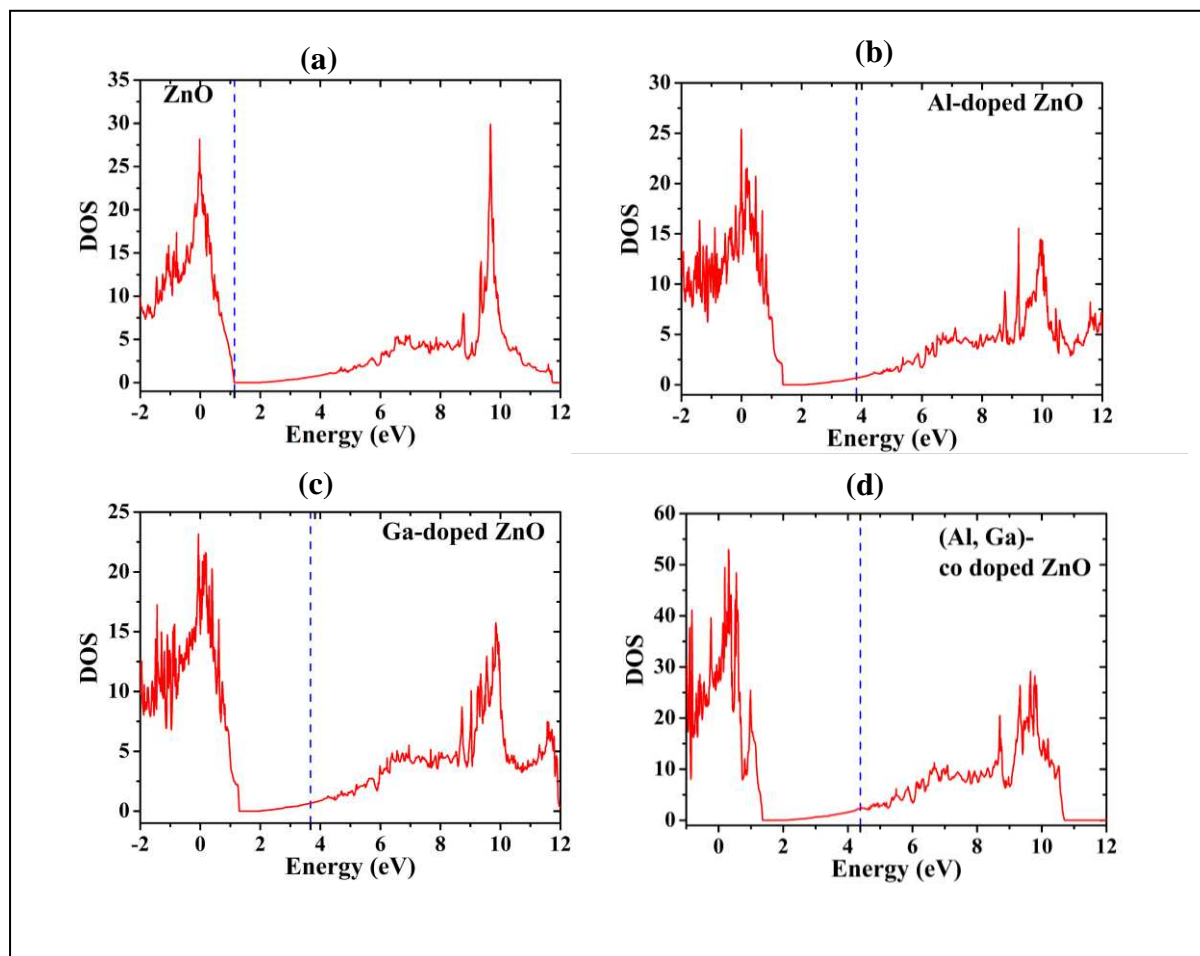


Fig. 7

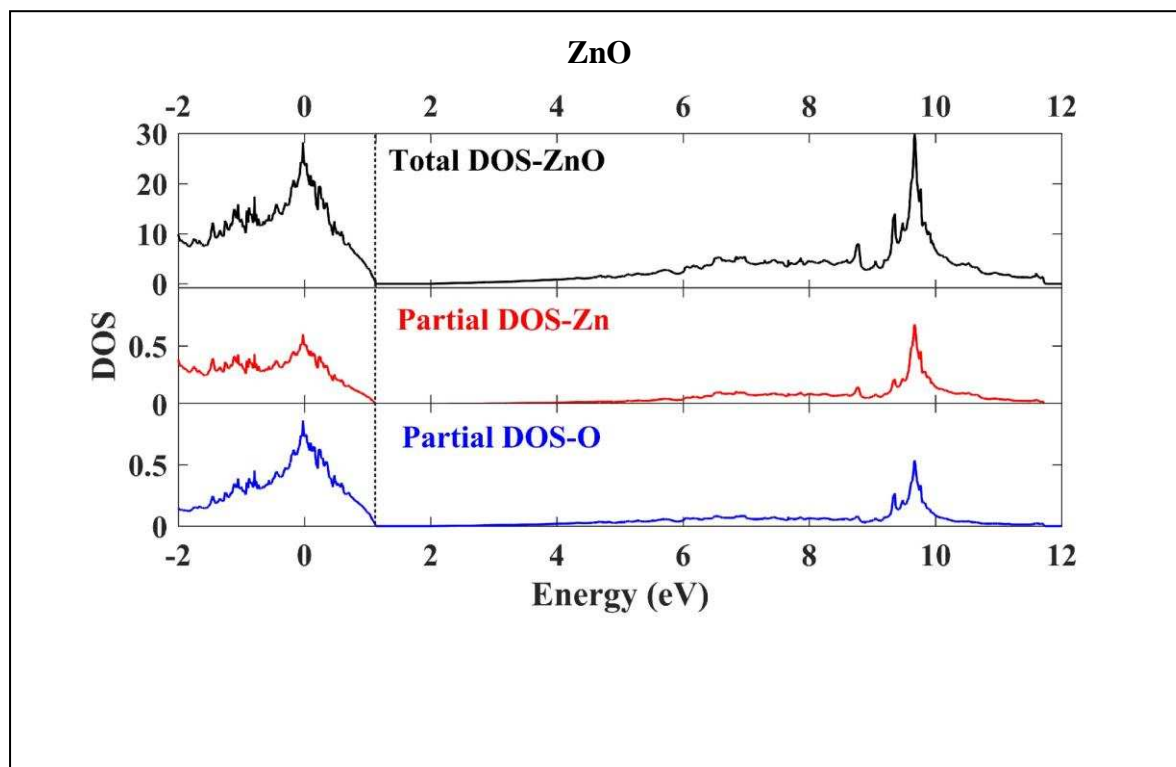


Fig. 8

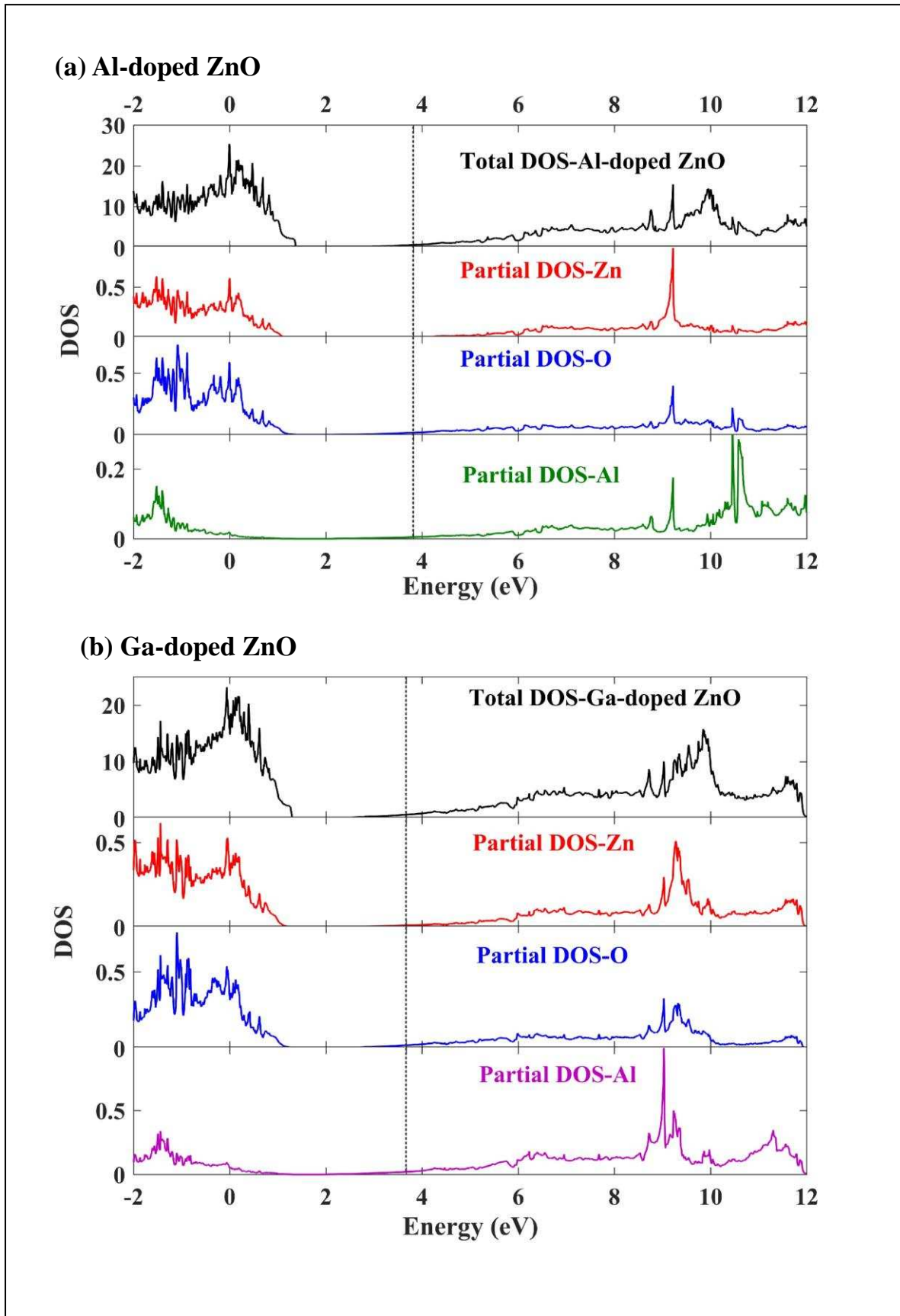


Fig. 9

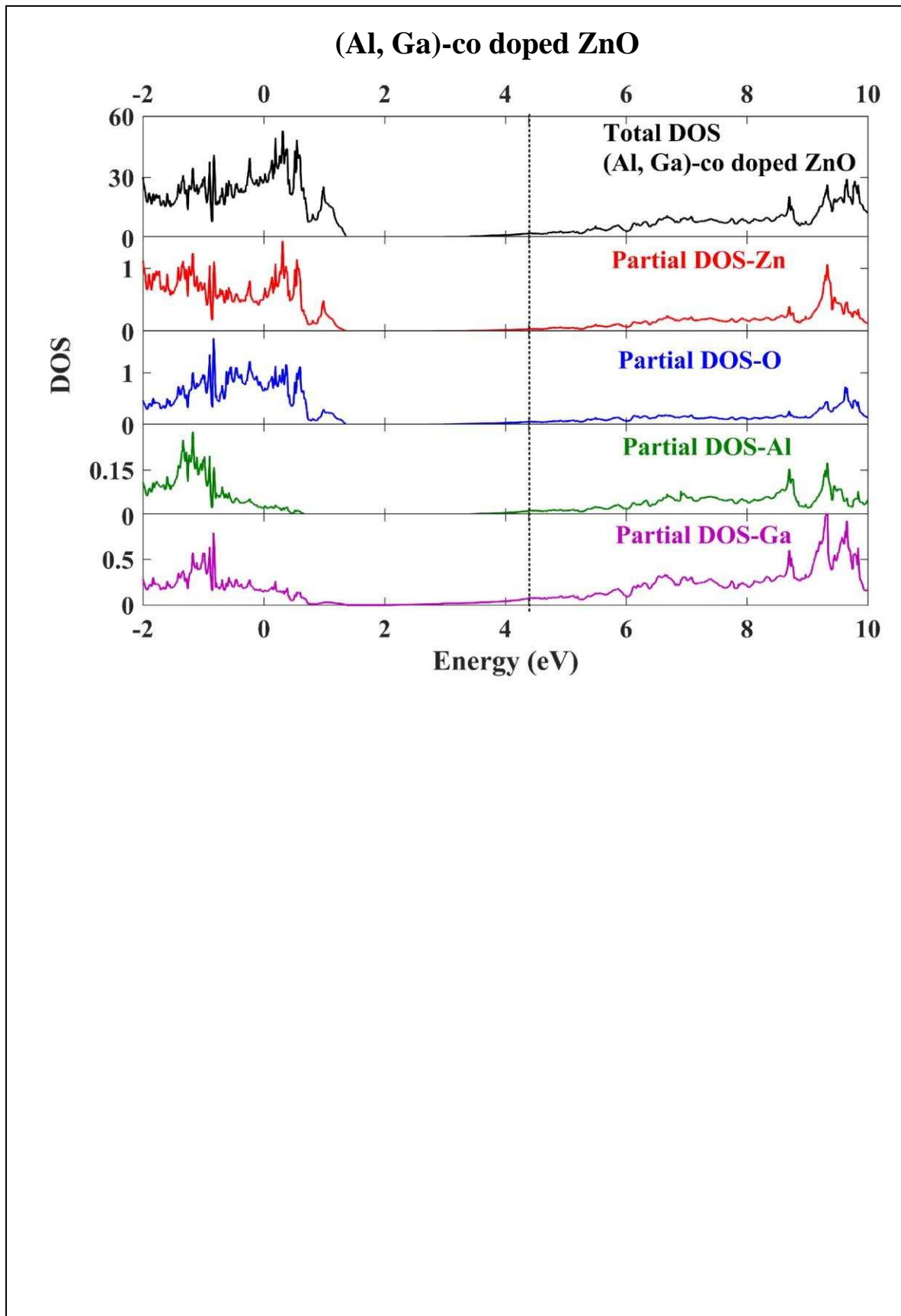


Fig. 10

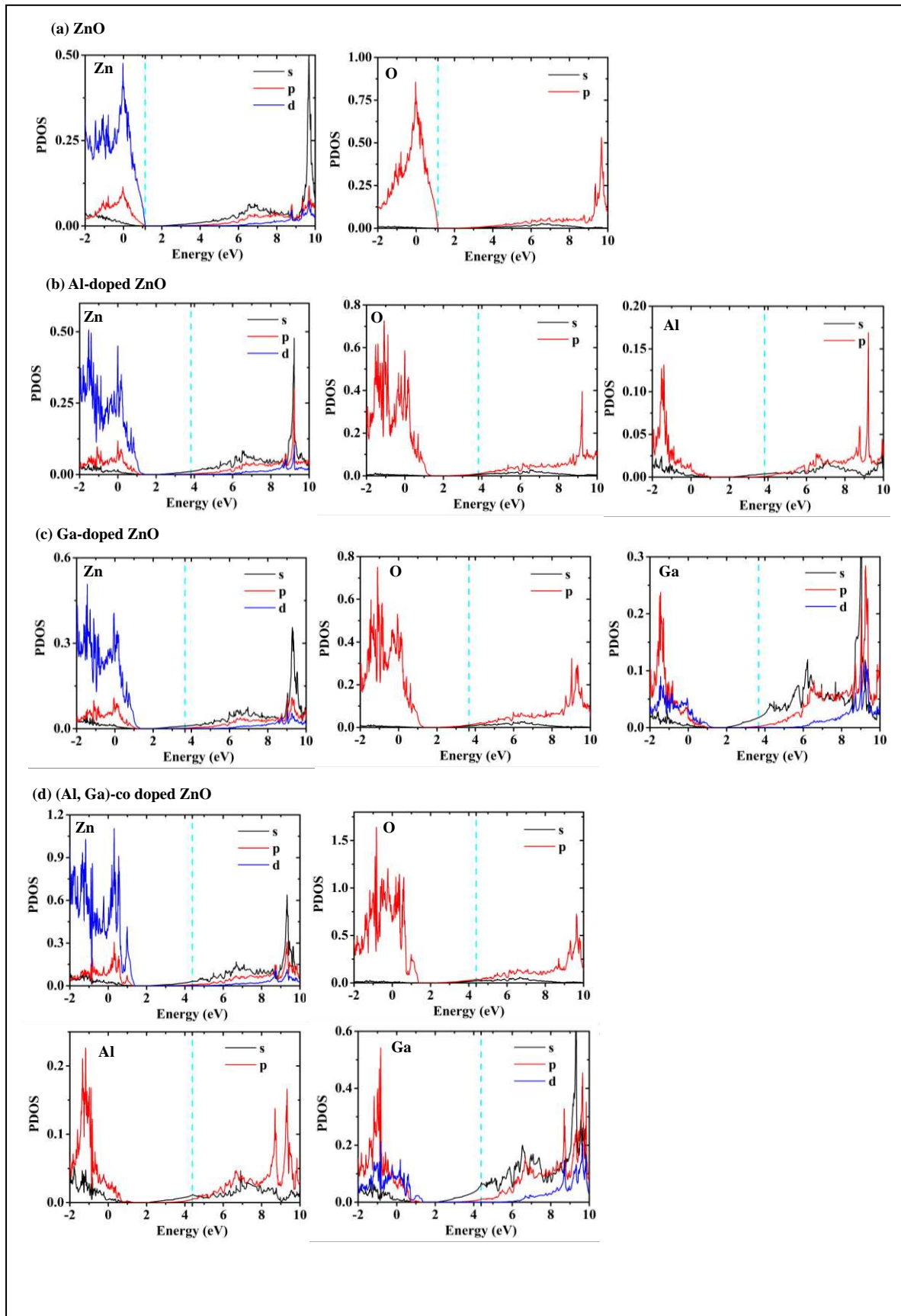


Fig. 11

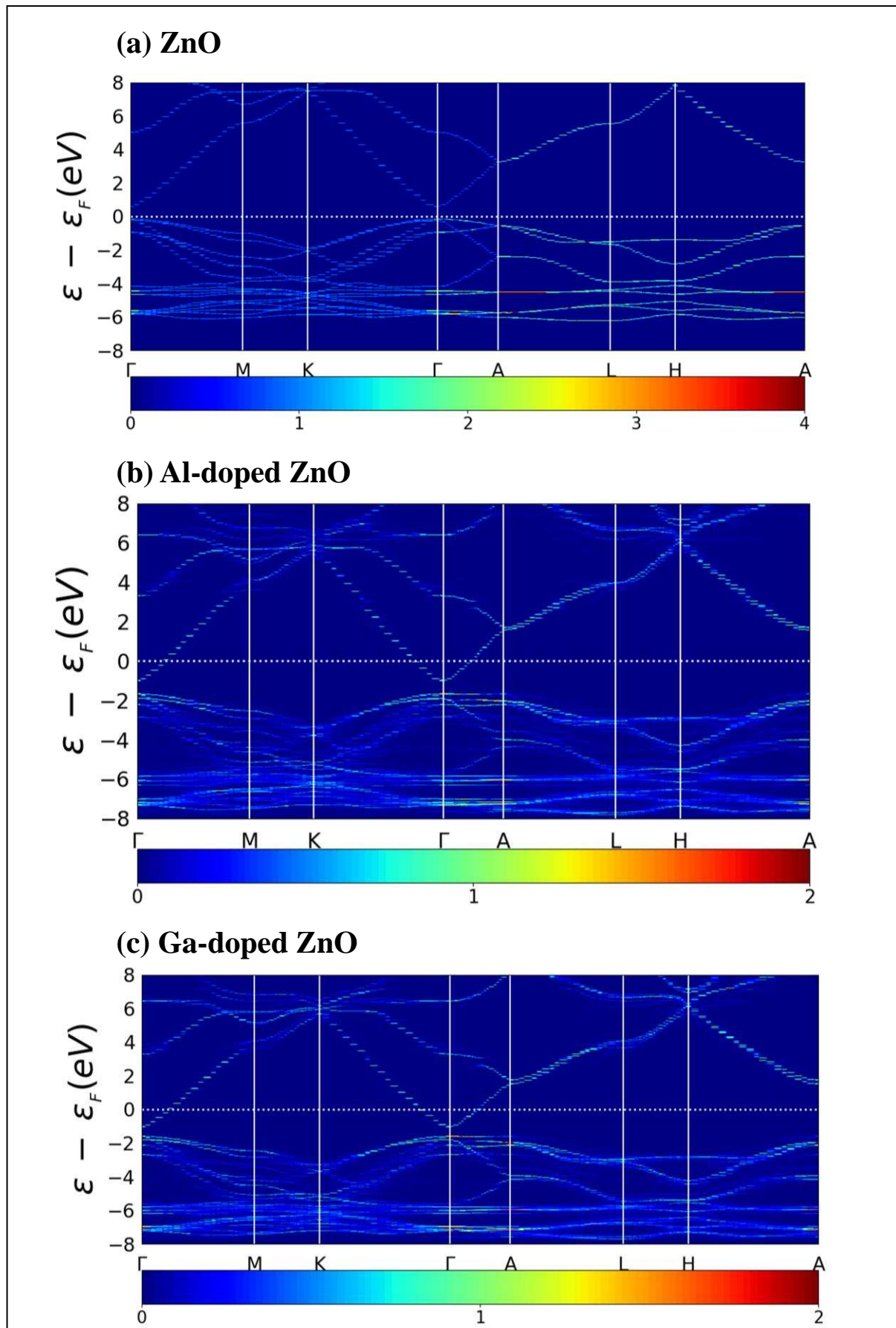


Fig. 12

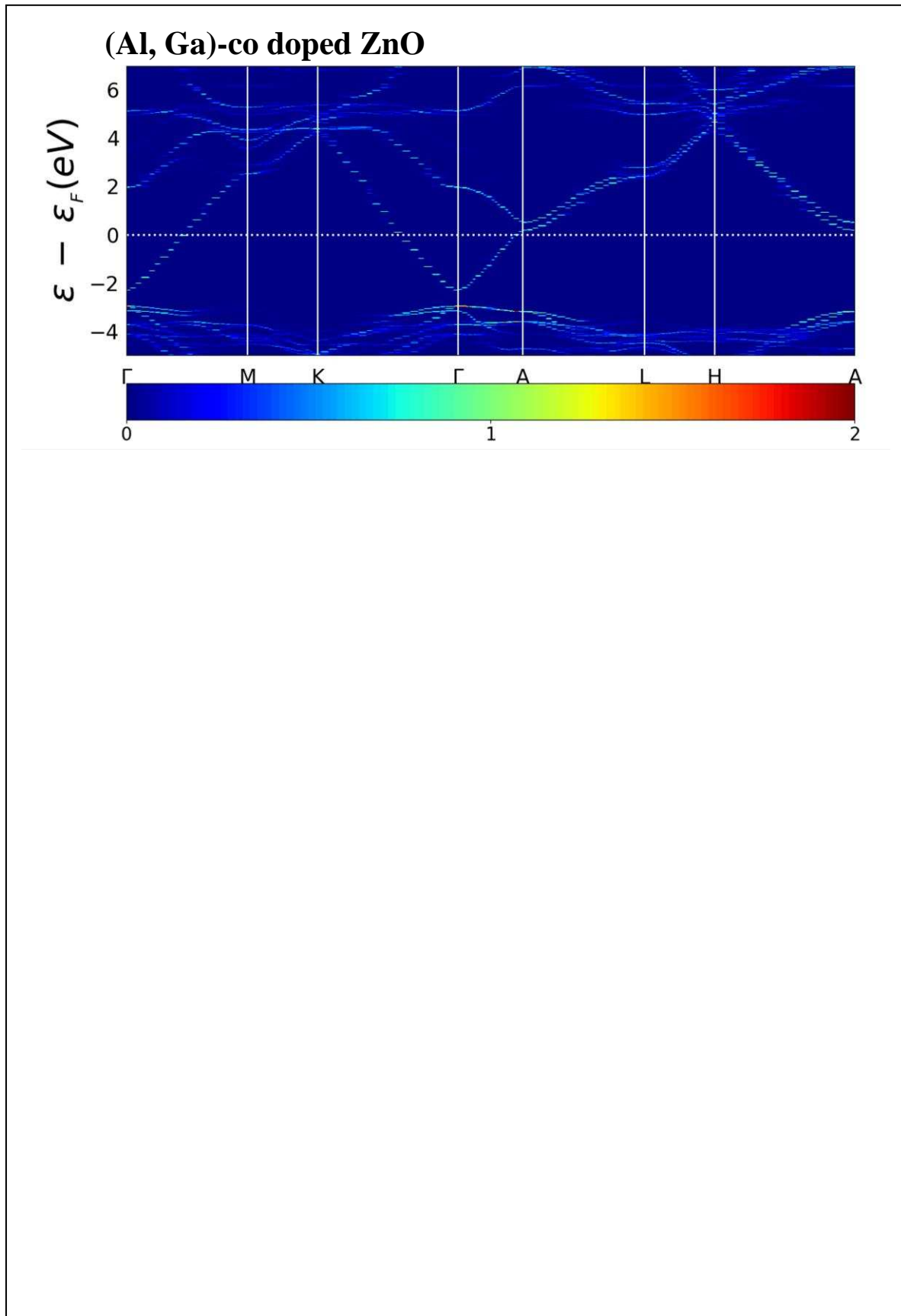


Fig. 13

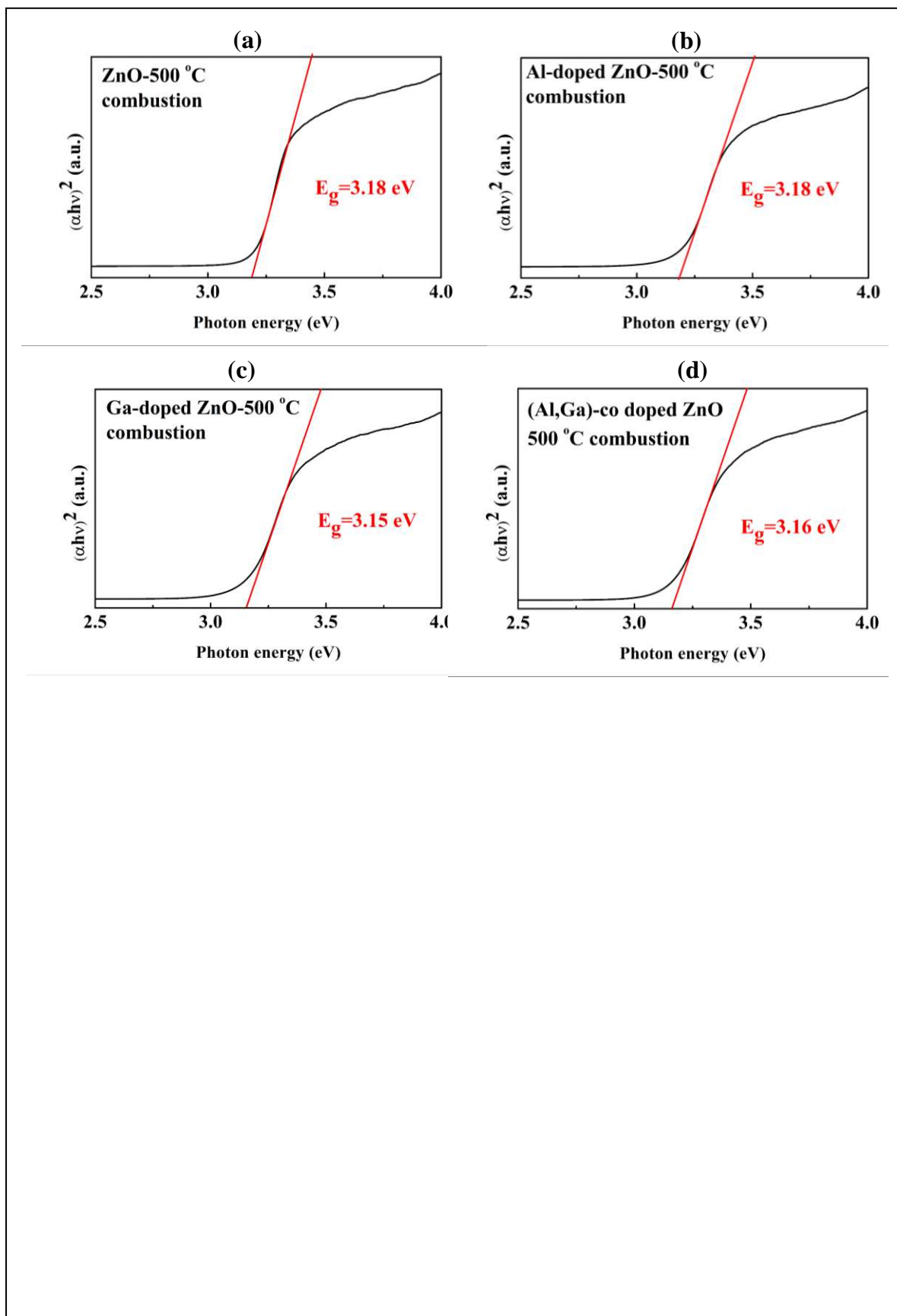


Fig. 14

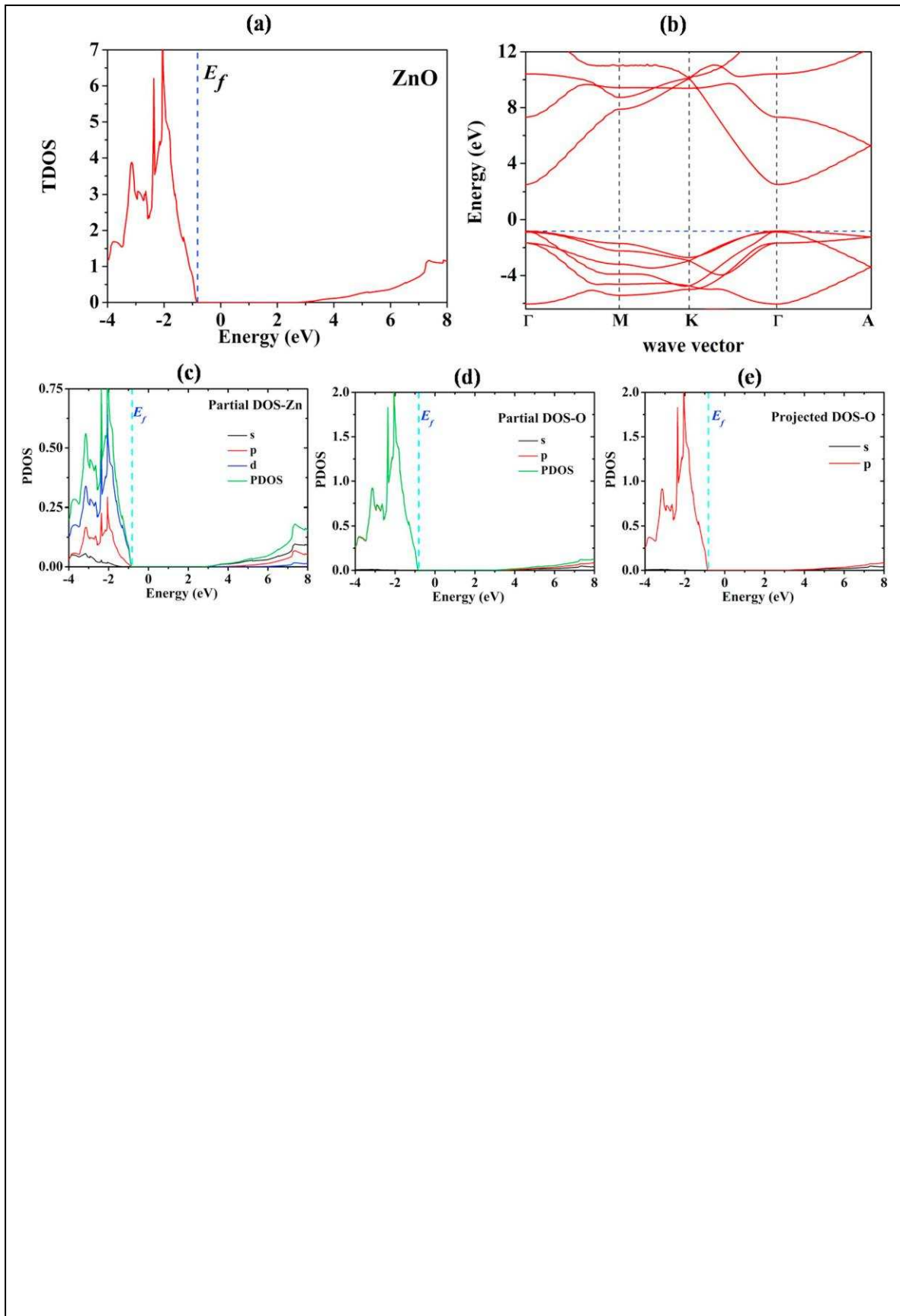


Fig. 15

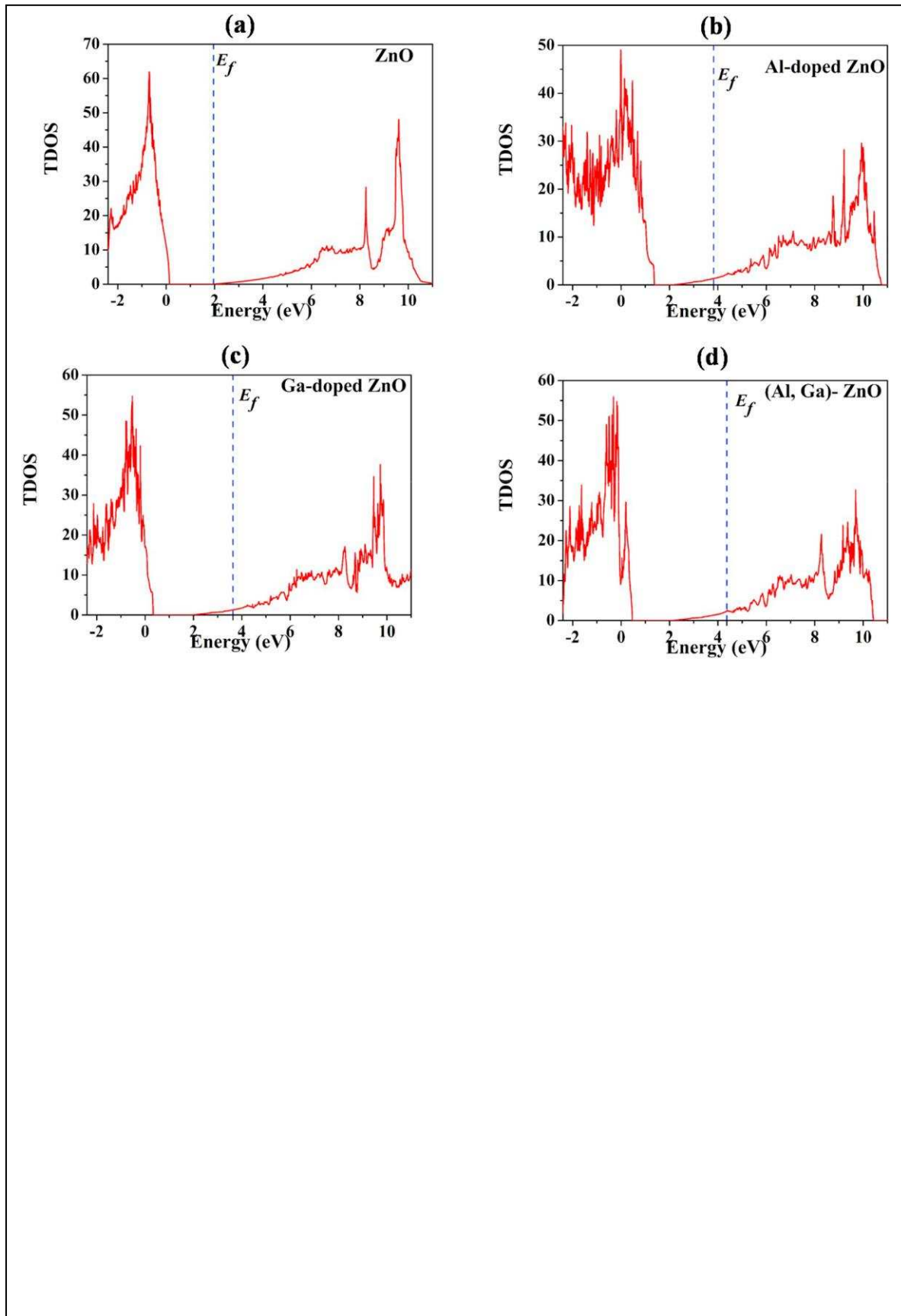


Fig. 16

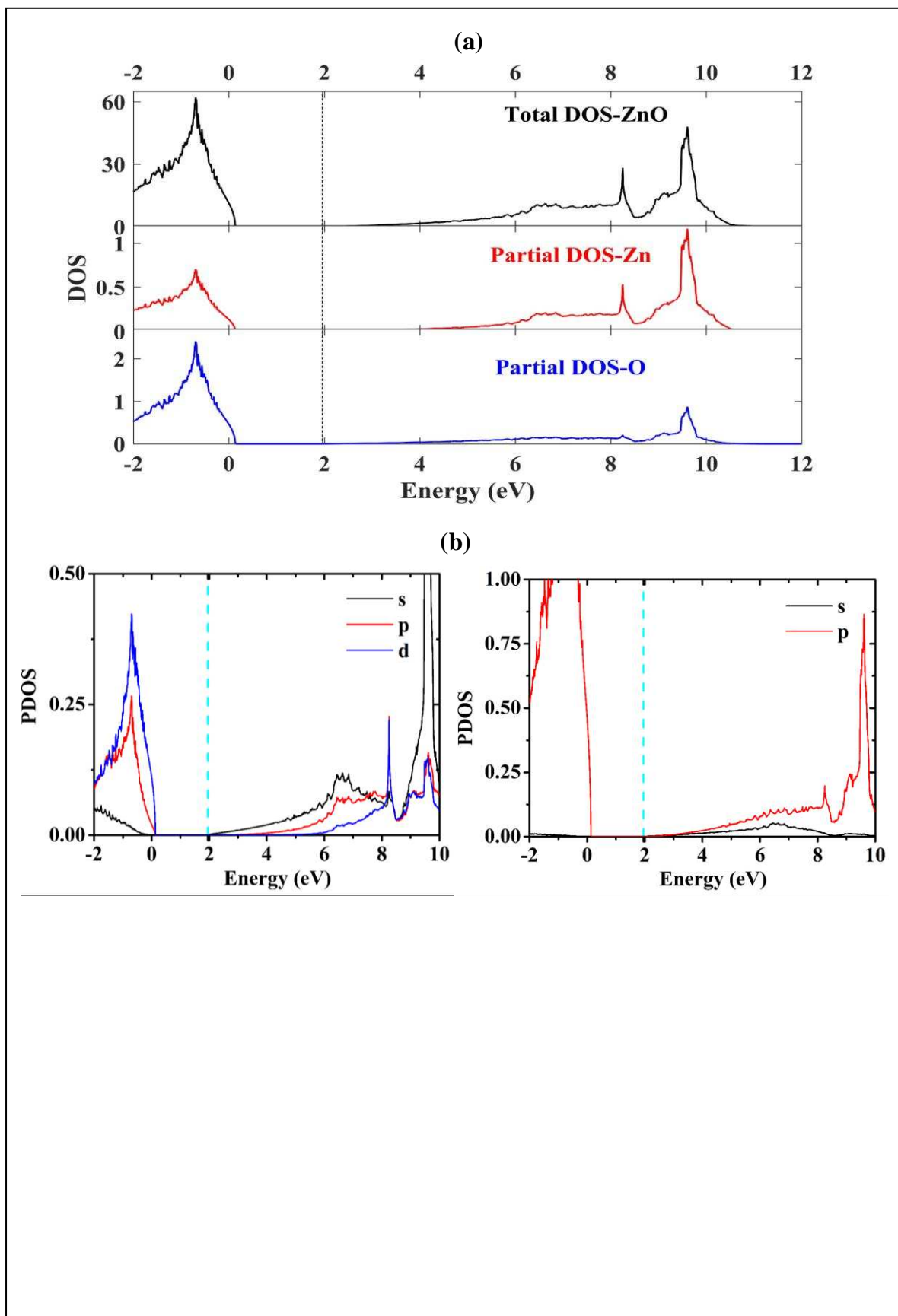


Fig. 17

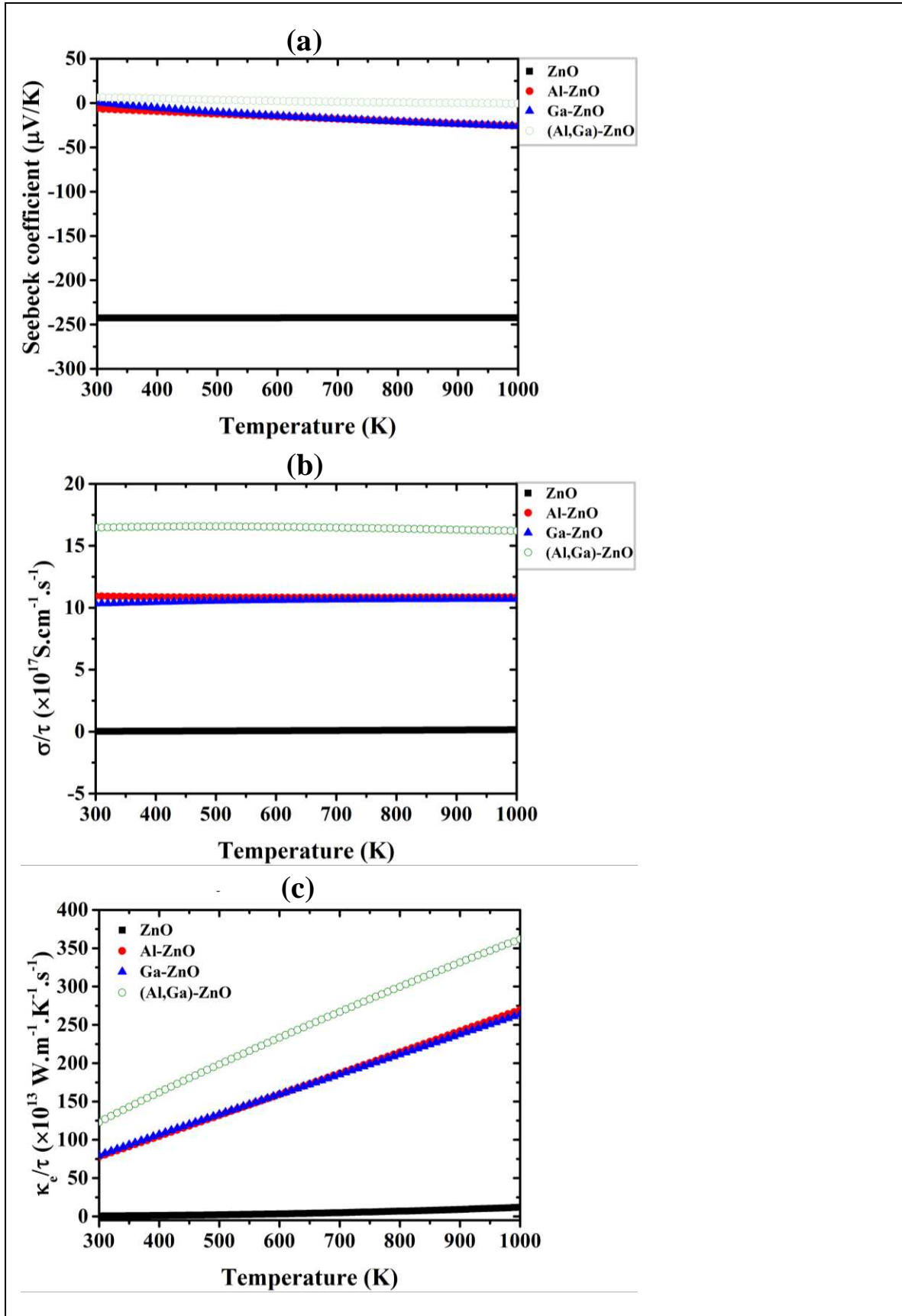


Fig. 18

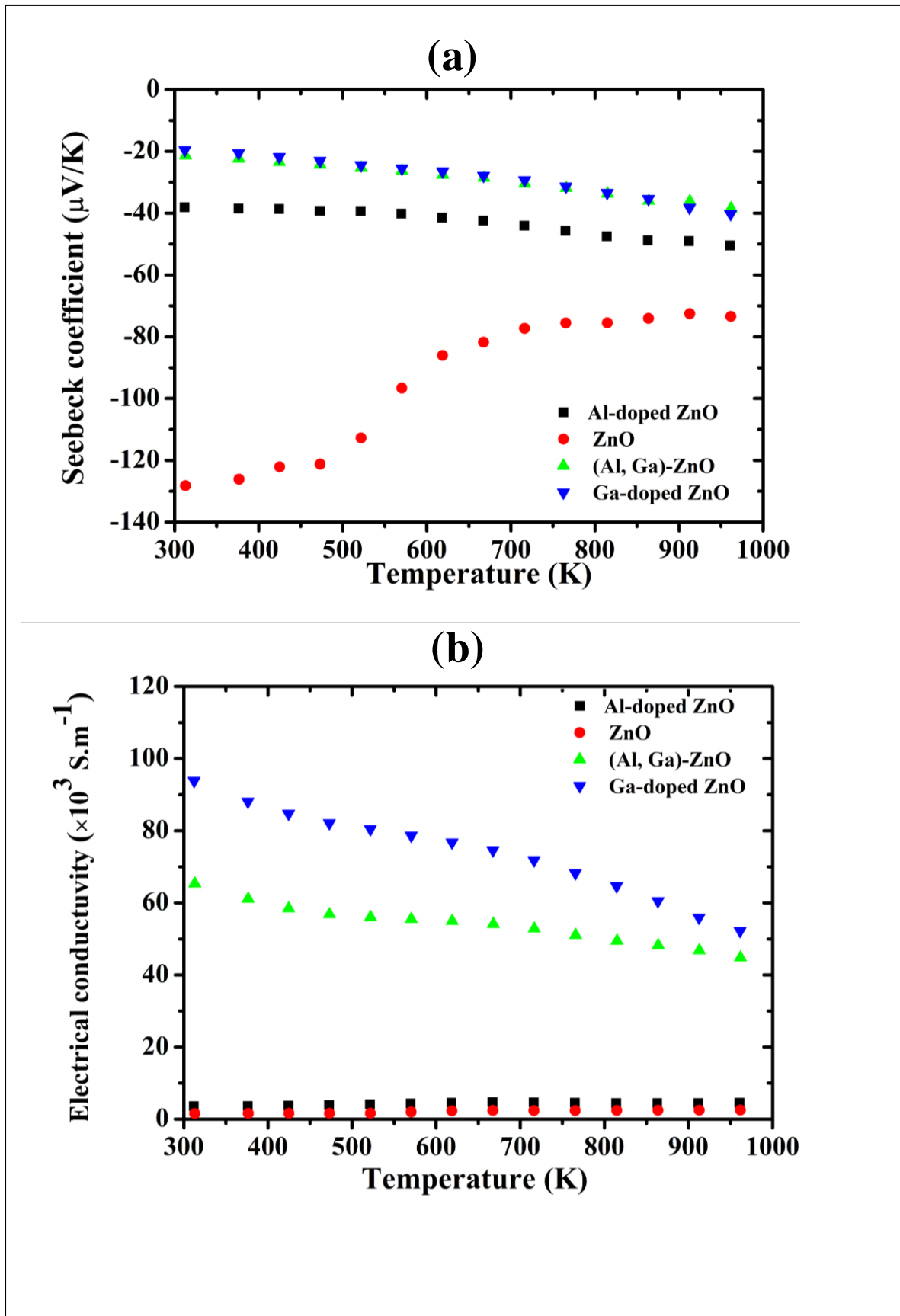


Fig. 19

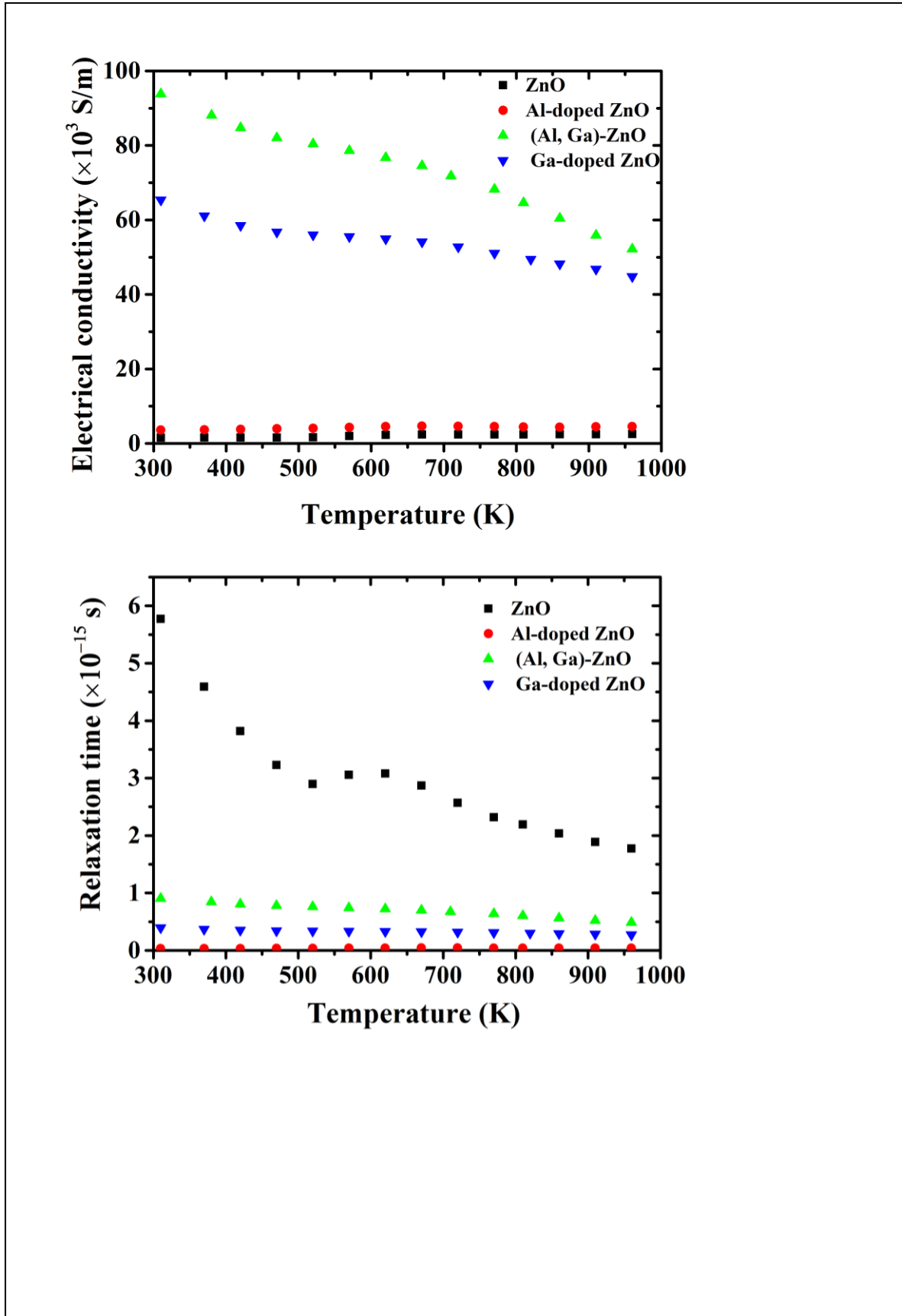


Fig. 20

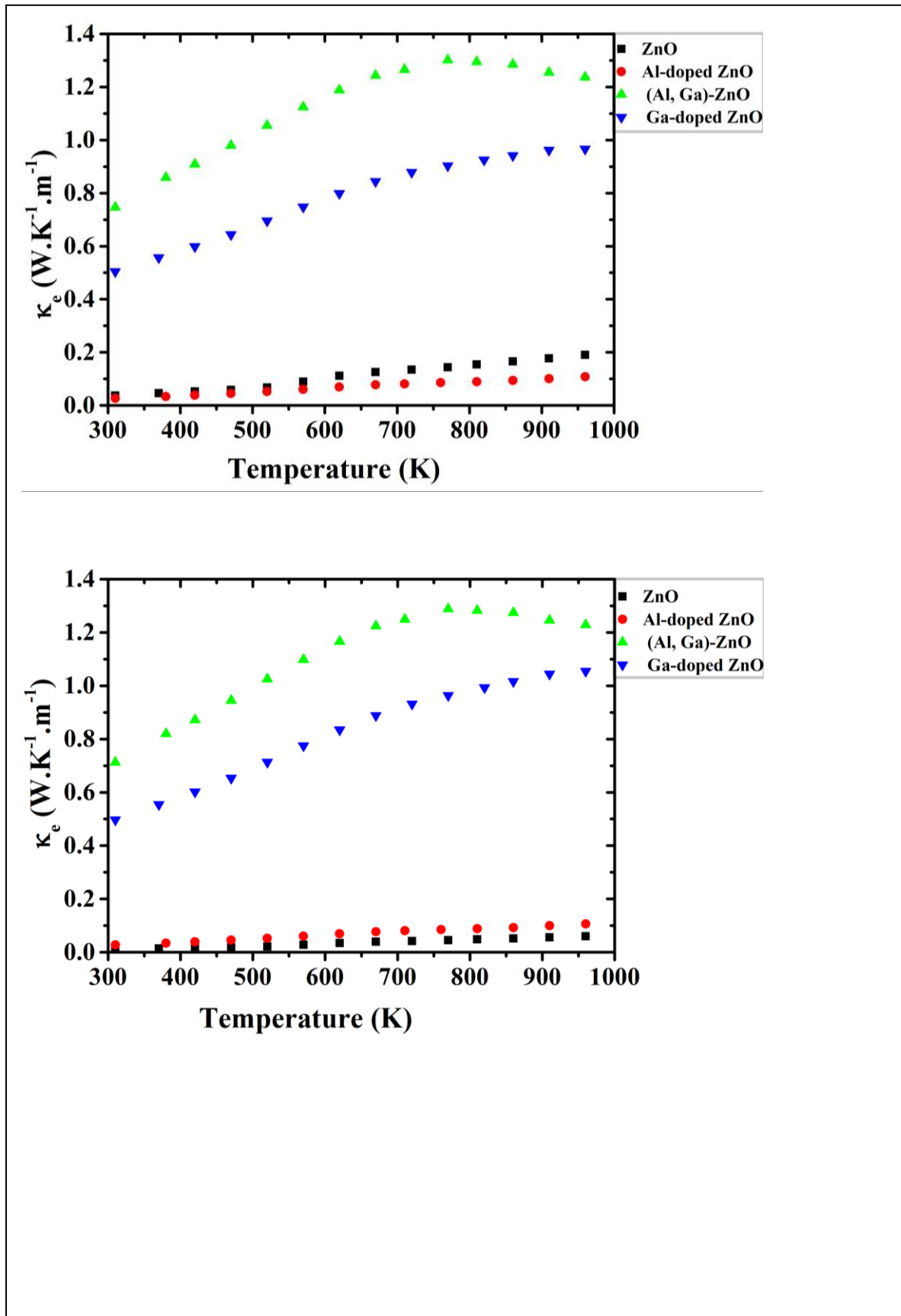


Fig. 21

